Simultaneous inhibition of the Arp2/3 complex and formins enhances *de novo* actin filament nucleation in Arabidopsis

Liyuan Xu[1], Lingyan Cao[1], Jiejie Li[1], Christopher J. Staiger[1,2,3,*]

[1] Department of Biological Sciences, Purdue University, West Lafayette, IN 47907, USA
[2] Department of Botany and Plant Pathology, Purdue University, West Lafayette, IN 47907, USA
[3] EMBRIO Institute, Purdue University, West Lafayette, IN 47907, USA

[*] Author for correspondence: staiger@purdue.edu

ORCID IDs: 0000-0001-9629-7133 (L.X.); 0000-0002-2906-1566 (J.L.); 0000-0003-2321-1671 (C.J.S.).

One sentence summary: Using advanced live-cell imaging and genetic mutation or small molecule inhibitor approaches, the roles for two classes of actin filament nucleator in maintaining the homeotic cortical cytoskeleton array are defined.

Running Title: Actin Filament Nucleation

Key words: actin cytoskeleton, Arp2/3 complex, formin, microscopy, nucleation factors

The author responsible for distribution of materials integral to the findings presented in this article in accordance with the policy described in the Instructions for Authors is: Christopher J. Staiger (staiger@purdue.edu)

Abstract

Precise control over how and where actin filaments are created in eukaryotic cells leads to the construction of unique cytoskeletal arrays with specific functions within a common cytoplasm. Actin filament nucleators are key players in this activity and include the conserved Actin-Related Protein 2/3 (Arp2/3) complex, that creates dendritic networks of branched filaments, as well as a large family of formins that typically generate long, unbranched filaments and bundles. In some eukaryotic cells, these nucleators compete for a common pool of actin monomers and loss of one favors the activity of the other. To test whether this is a common mechanism across kingdoms, we combined the ability to image single filament dynamics in the homeostatic cortical actin array of living Arabidopsis (*Arabidopsis thaliana*) epidermal cells with genetic and/or small molecule inhibitor approaches to stably or acutely disrupt nucleator activity. We found that Arp2/3 mutants or acute CK-666 treatment markedly reduced the frequency of side-branched nucleation events as well as overall actin filament abundance. We also confirmed that plant formins contributed to side-branched filament nucleation. Surprisingly, simultaneous inhibition of both nucleators increased overall actin filament abundance and enhanced the frequency of *de novo* nucleation events. Collectively, these observations suggest that plant cells have a unique actin filament nucleation mechanism that maintains cortical actin organization and dynamics when compared to yeast or animal cells.

Introduction

The actin cytoskeleton comprises a dynamic network of filaments that participates in a wide variety of cellular activities including vesicle/organelle trafficking, cell expansion, cellulose synthesis, tissue/organelle development, and resistance to microbial pathogen invasion (Gao et al., 2009; Sampathkumar et al., 2013; Peremyslov et al., 2015; Scheuring et al., 2016; Qi and Greb, 2017; Li and Staiger, 2018; Zhang et al., 2019). Plant cells rearrange their actin cytoskeleton organization on timescales of seconds to minutes in response to biotic or abiotic stimuli, which means the actin cytoskeleton organization is extremely dynamic but also precisely controlled (Staiger et al., 2009; Henty-Ridilla et al., 2013b). Regulation of the cytoskeleton involves dozens of actin-binding proteins (ABPs) that participate in filament nucleation, elongation, severing, and depolymerization. Nucleators initiate the formation of new actin filaments at a much faster rate than spontaneous nucleation from actin monomers and are therefore considered key regulators of array formation and actin dynamics (Kadzik et al., 2020; Rosenbloom et al., 2021). Previous in-vitro studies demonstrate that the actin nucleation pathway utilizes both the Actin-Related Protein 2/3 (Arp2/3) complex and formins, two distinct actin filament nucleators with different specific activation mechanisms (Kovar, 2006; Pollard, 2007; Paul and Pollard, 2008; Burke et al., 2014; Suarez et al., 2015).

The Arp2/3 complex is a seven-subunit protein complex responsible for generating branched actin filaments and forming dendritic actin networks in eukaryotic cells (Mullins et al., 1998; Pollard, 2007). Once the Arp2/3 complex gets activated, the ARP2 and ARP3 subunits along with a recruited actin monomer can nucleate the polymerization of a new (daughter) filament, which grows from the side of a pre-existing (mother) actin filament with a characteristic 70° angle (Mullins et al., 1998; Dayel and Mullins, 2004; Pollard, 2007; Beltzner and Pollard, 2008; Rouiller et al., 2008). This branched actin network structure is critical for many cellular processes in yeast and animal cells, such as cell division, cell migration, exocytosis, endocytosis and tissue or embryo development (Roh-Johnson and Goldstein, 2009; Cabrera et al., 2011; Sun et al., 2013; van der Kammen et al., 2017). In contrast, plants, such as Arabidopsis, with mutations in Arp2/3 subunits have relatively normal morphology and fertility; however, these Arp2/3 mutants have marked defects in epidermal cell morphology including distorted trichomes, cell-cell adhesion defects, and fewer lobes on leaf pavement cells (Szymanski et al., 1999; Le et al., 2003; Li et al., 2003; Mathur et al., 2003a; Harries et al., 2005; Yanagisawa et al., 2015). Recent research shows that plant Arp2/3 complex is also involved in auxin transport (Peng et al., 2017; Sahi et al., 2018; García-González et al., 2020),

guard cell opening and closing (Jiang et al., 2012; Li et al., 2014), resistance to penetration-mediated infection by fungal pathogens (Qin et al., 2021), and possibly in autophagy (Wang et al., 2016; Wang et al., 2019). Many of these studies also reveal that *arp2/3* mutant cells have reduced actin filament abundance or misaligned actin bundles, which suggests that these functions of the Arp2/3 complex may be accomplished through regulating specific actin structures. In growing trichome branches, for example, the Arp2/3 complex generates a tip-localized actin filament array constrained by cortical microtubules that coordinates growth (Yanagisawa et al., 2015; Yanagisawa et al., 2018). During fungal invasion, the Arp2/3 complex localizes to the site of penetration peg attack in epidermal pavement cells and generates a large cortical actin filament patch necessary to suppress invasion (Qin et al., 2021). However, the molecular mechanisms by which the Arp2/3 complex coordinates the organization of cortical actin filament arrays in unstimulated cells or how it generates unique arrays in response to biotic and abiotic stress are poorly understood.

Another family of evolutionarily conserved actin filament nucleators are the formins that typically generate long linear actin filaments that can bundle together to form actin cables (Kovar, 2006; Pollard, 2007; Paul and Pollard, 2008). These actin cables provide tracks for intracellular organelle/vesicle trafficking. Formins have two universally conserved formin-homology domains, FH1 and FH2. The proline-rich FH1 domain allows formins to recruit profilin-bound actin to elongate actin filaments at the barbed ends. The FH2 domain, on the other hand, interacts with other regions within itself for autoinhibition or it can interact with the FH2 domain of another formin to form a dimer, which initiates the nucleation of linear actin filaments (Cvrčková et al., 2000; Deeks et al., 2002; Cheung and Wu, 2004; Cvrčková et al., 2004; Kovar, 2006; Michelot et al., 2006; Pollard, 2007; Paul and Pollard, 2008). There are 21 formin homologs in Arabidopsis and these are separated into two different phylogenetic subclasses (Cvrčková et al., 2000). Based on sequence prediction, Class I formins have a signal peptide and an N-terminal transmembrane domain that target them to the plasma membrane, whereas Class II formins are predicted to have more diverse domain structures (Cvrčková et al., 2000; Deeks et al., 2002; Cheung and Wu, 2004; Cvrčková et al., 2004; Michelot et al., 2006). In addition, plant formin orthologs can be categorized with respect to how they generate actin filaments. Processive formins remain attached to the actin filament barbed end and move processively as the filament elongates, whereas non-processive formins remain at the filament nucleation site (Cvrčková et al., 2000; Deeks et al., 2002; Cheung and Wu, 2004; Cvrčková et al., 2004; Michelot et al., 2006). Biochemical results reveal that a non-processive Class I formin,

FORMIN1 (AFH1), attaches to the side of a pre-existing actin filament to nucleate new filaments, which suggests a far more complicated role for formins in plant cells than just generating linear filaments (Michelot et al., 2006). In addition, both in vivo and in vitro experiments showed that formins are critical for maintaining homeostatic actin array organization as well as regulating polarized cell growth (Vidali et al., 2009; Rosero et al., 2013; Lan et al., 2018). However, the detailed molecular mechanism of how formins regulate actin structure and single actin filament dynamics in plant cells remains unclear.

The decision of when and where to generate an actin array as well as its specific structure and size is essential for each actin array to specifically choreograph its cellular function and often requires coordination between the Arp2/3 complex and formins. Studies in fission yeast and some animal cells indicate that the Arp2/3 complex and formins compete for a limited supply of actin monomers and this competition prevents excessive activity of one or the other, thereby allowing cells to generate distinct actin structures and dynamics by regulating the balance of activities between these two nucleators (Hotulainen and Lappalainen, 2006; Lomakin et al., 2015; Suarez et al., 2015; Davidson et al., 2018; Antkowiak et al., 2019; Chan et al., 2019; Kadzik et al., 2020). During actin array assembly, the Arp2/3 complex generates branched filament arrays whereas formins produce linear filament bundles (Carlier and Shekhar, 2017). Furthermore, in-vitro studies reveal that filaments generated by formin grow faster than Arp2/3-nucleated ones (Vavylonis et al., 2006; Michelot et al., 2013; Suarez et al., 2015; Funk et al., 2019). Studies with M2 melanoma cells and HeLa cells illustrate that actin filaments generated by different nucleators have distinct properties for filament abundance, filament length, and turnover kinetics, but that both nucleators contribute to maintenance and turnover of the homeostatic actin cortex (Fritzsche et al., 2016). A recent study in *Arabidopsis* shows that actin arrays in cotyledon epidermal pavement cells are slightly more dense and the extent of bundling is unchanged when either a Class I formin, AFH1, or the Arp2/3 subunit, ARPC5, are genetically down-regulated; however, single filament dynamics or nucleation events were not evaluated directly (Cifrová et al., 2020). The authors propose that the Arp2/3 complex and formins in plants may have complementary roles to overcome the loss of one or the other. Nevertheless, the underlying mechanism of filament nucleation and the nature of the actin arrays that each nucleation factor constructs remain to be fully elucidated. Therefore, it is important to understand how each nucleator regulates the structure and dynamic properties of actin arrays individually in order to better understand how they contribute to the cortical actin

homeostasis and how they are coordinated to regulate the actin cytoskeleton during different biological processes.

Quantitative analysis of single actin filament dynamics in vivo is relatively hard to conduct in yeast and mammalian cells, because either the cells are too small or the actin arrays are too dense and filament lengths are below the limits of resolution of light microscopy. Epidermal cells from dark-grown Arabidopsis hypocotyls are large in size and have relatively sparse actin arrays in the cortical cytoplasm, making this a powerful model system for quantitative analysis of single actin filament dynamics, especially when combined with high spatial and temporal resolution imaging approaches and genetically-encoded fluorescence reporters (Staiger et al., 2009; Henty et al., 2011; Henty-Ridilla et al., 2013a; Cai et al., 2014; Cao et al., 2016; Arieti and Staiger, 2020). Previous work demonstrates a remarkably high rate of new filament construction, rapid growth at filament ends, and disassembly by prolific severing activity in a mechanism termed “stochastic dynamics” (Staiger et al., 2009). The ability to observe both actin filament architecture and activities of single filaments in living cells allows direct visualization of the effects associated with the disruption of actin nucleators on filament activities in vivo (Cao et al., 2016).

In this study, we test the hypothesis that the Arabidopsis Arp2/3 complex mediates nucleation of side-branched filaments in vivo but does not facilitate filament elongation directly. We used both genetic and pharmacological approaches to disrupt Arp2/3 complex activity in plant cells. With quantitative live-cell imaging at single filament resolution, we demonstrated that the Arp2/3 complex is responsible for the nucleation of side-branched filaments. We also characterized the difference between the Arp2/3 complex and formins with respect to the dynamic behaviors of the filaments they generate and evaluated the consequence of losing both classes of filament nucleator on actin organization and dynamics. Surprisingly, living plant cells deficient for two classes of nucleator generate comparatively normal and dynamic actin arrays by an apparent *de novo* filament nucleation mechanism.

Results

Arabidopsis plants have defects in general growth and epidermal cell morphology when deficient for the Arp2/3 complex

Previous studies of Arp2/3 complex mutants reveal defects in Arabidopsis epidermal cell growth and morphology (Szymanski et al., 1999; Le et al., 2003; Li et al., 2003; Mathur et al., 2003b; Harries et al., 2005; Facette et al., 2015; Yanagisawa et al., 2015; Cifrová et al., 2020). Here, we acquired a homozygous T-DNA insertion mutant for *ARP2*, *arp2-1* (or *wrm1-2*; SALK_003448), and a point mutation of *ARPC2*, *arpc2* (or *dis2-1*; El-Assal et al., 2004), and confirmed the cell and organ growth phenotypes. We confirmed that both *arp2-1* and *arpc2* homozygous mutant plants had adhesion defects at end walls of hypocotyl epidermal cells and severely distorted leaf trichomes when compared to wild-type sibling lines (Figure 1A). In addition, hypocotyls of *arp2-1* and *arpc2* were significantly shorter than wild-type seedlings at the same time points (Figure 1, B and C). To test whether hypocotyl growth defects resulted from defects in cell expansion, we examined epidermal cell length and found that cells in all regions of etiolated *arp2/3* hypocotyls were significantly shorter compared to wild-type hypocotyls; however, cell widths were not affected (Figure 1, D and E). Similar results for root growth were observed in light-grown seedlings (Figure 1, F and G). These results confirm that the Arp2/3 complex plays a role in axial cell expansion in both dark-grown hypocotyls and light-grown roots of Arabidopsis.

Actin filament abundance and bundling are reduced in *arp2/3* mutants

To assess the influence of the Arp2/3 complex on cortical actin cytoskeletal organization, we compared images of epidermal cells from the apical region of 5-d-old etiolated wild-type, *arp2-1,* and *arpc2* hypocotyls collected by variable-angle epifluorescence microscopy (VAEM) (Staiger et al., 2009). Homozygous mutant and isogenic wild-type sibling lines that express the actin reporter, green fluorescent protein (GFP) fused with FIMBRIN1 actin-binding domain 2 or GFP-fABD2 (Sheahan et al., 2004) were prepared by crossing to facilitate observation and measurement of the organization and filament dynamics of the actin cytoskeleton (Staiger et al., 2009). The actin array structure in *arp2-1* and *arpc2* cells had fewer, thinner, and more scattered filaments compared to corresponding wild-type cells (Figure 2A). To compare these differences quantitively, we used *density*, *skewness, angle*, and *parallelness* as four key parameters established previously for standardized descriptions of actin cytoskeleton array organization in living cells (Higaki et al., 2010; Ueda et al., 2010; Henty et al., 2011; Li et al.,

2012; Cai et al., 2014; Cao et al., 2016; Arieti and Staiger, 2020). Density measures the percentage of occupancy of actin filaments, skewness defines the extent of bundling of actin filaments, and angle and parallelness describe how filaments orient relative to the longitudinal axis of the cell or each other, respectively. Actin density in *arp2-1* and *arpc2* cells was significantly decreased compared to the respective wild-type cells (Figure 2B), and the extent of filament bundling was significantly reduced as well (Figure 2C). The average angle of filament arrays was not significantly different between *arp2-1*, *arpc2,* and wild-type cells (Figure 2D). The population distribution of filament parallelness in *arp2-1* and *arpc2* was left-skewed compared to that in the wild type, indicating that filaments were more parallel to each other in *arp2/3* mutant cells; however, the mean values were not significantly different between any of these genotypes (Figure 2E). These results demonstrate that the Arp2/3 complex contributes to the generation of both individual filaments and filament bundles and is necessary for maintaining homeostatic organization of the cortical actin cytoskeleton in epidermal cells.

The Arp2/3 complex plays a significant role in filament nucleation and generation of side-branched filaments

To investigate how the Arp2/3 complex participates in actin filament nucleation, we measured single actin filament formation and dynamics in wild-type and *arp2/3* mutant cells by collecting time-lapse movies from the apical regions of 5-d-old dark-grown hypocotyls with VAEM. The sparse nature of the cortical actin array in hypocotyl epidermal cells and the high spatial and temporal resolution afforded by VAEM allowed us to visualize (Figure 3A) and quantify individual nucleation events by a previously described assay (Cao et al., 2016). Briefly, we counted all new or regrowing filaments identified in multiple 400 μm^2 regions of interest (ROI) within a cell during a 100-s time-lapse movie. The nucleation frequency was normalized to the average filament number within each ROI to minimize the influence of filament abundance differences between ROIs and genotypes. The overall nucleation frequency in *arp2-1* cells (0.36 ± 0.03 events/filament/min) was significantly decreased compared to wild-type cells (0.61 ± 0.03 events/filament/min) (Figure 3B; Supplemental Movie S1; Supplemental Movie S2) and coincided with our observation that loss of function of the Arp2/3 complex resulted in a significant reduction in filament abundance (Figure 2B). Similar reductions in overall nucleation frequency were also observed for *arpc2* compared to wild-type cells (Supplemental Figure S1A). Next, we classified nucleation events into three different subpopulations based on filament origin: *de novo* from the cytoplasm; from the side of a pre-existing filament or bundle; or, from the end of a pre-existing filament (Figure 3A; Supplemental Movies S3 to S5) (Staiger et al.,

2009; Henty-Ridilla et al., 2013a; Cao et al., 2016). Only the side-branched nucleation frequency was significantly decreased in *arp2-1* and *arpc2* cells compared to the respective wild-type sibling cells (Figure 3C; Supplemental Movies S1 and S2; Supplemental Figure S1A). Side-branched nucleation events contribute about half of all new filament origins and these were reduced by 60–70% in the *arp2/3* mutants.

To understand how the Arp2/3 complex influences the dynamics of actin filaments, we tracked many dozens of individual filaments from their first appearance to complete disappearance and measured several parameters that were previously established to describe actin filament turnover (Figure 4A; Table 1; Supplemental Movies S6 and S7). Compared to wild type, the population distribution of actin filament elongation rates in *arp2-1* cells was more left skewed, and the average filament elongation rate was also higher (Figure 4B; Table 1), indicating that actin filaments were growing significantly faster in *arp2-1* cells. It is also obvious that there were two or three distinct populations of filament elongation rates with peaks at 0.75 – 1.25, 2.0 – 2.25, and > 3 μm/s with the latter two categories becoming more prevalent in *arp2-1* cells (Figure 4B). Similar differences in overall elongation rate and fast-growing filament populations were observed in *arpc2* (Supplemental Table S1; Supplemental Figure S1E). Filaments in both *arp2-1* and *arpc2* mutant cells also had significantly longer filament length and lifetimes than the ones in respective wild-type cells (Table 1; Supplemental Table S1).

Previous in vitro data suggest that filament ends generated by the Arp2/3 complex and formins have different elongation rates; many formins are processive polymerases that use profilin-actin to add monomers to growing filaments (Kovar et al., 2003; Romero et al., 2004; Akin and Mullins, 2008). To test whether dynamic properties of filaments with different nucleation patterns are distinct from each other, we measured the full suite of dynamic parameters for each population. We found that side-branched filaments in *arp2-1* cells were significantly longer (Figure 4C) and filament lifetime was prolonged (Figure 4D) compared to the side-branched filaments in wild-type cells; in addition, the filament severing frequency was slightly reduced in *arp2-1* cells (Figure 4E). These dynamic differences between side-branched filaments in *arpc2* mutant and wild-type sibling cells were conserved (Supplemental Figure S1).

Collectively, these data demonstrate that the Arp2/3 complex is responsible for generating new filaments from the side of pre-existing filaments and is necessary for cells to maintain the homeostatic actin cytoskeleton architecture. Moreover, Arp2/3-nucleated filaments have distinct dynamic properties compared with those generated *de novo* or from the end of a

pre-existing filament; in particular, they grow slower and are shorter, and have reduced filament lifetimes.

The small molecule inhibitor CK-666 phenocopies actin-based defects in *arp2* and *arpc2* mutants

Recent studies show that CK-666, a small molecule inhibitor of the Arp2/3 complex that is effective on yeast and animal cells (Nolen et al., 2009; Hetrick et al., 2013), phenocopies the effects of *arp2/3* mutants on tomato pollen tube growth (Liu et al., 2020) and *Arabidopsis* sperm nuclear migration (Ali et al., 2020), both of which depend upon the actin cytoskeleton. Although the latter studies did not directly demonstrate the effects of CK-666 on actin structure or filament nucleation, they do suggest that CK-666 could be a potential Arp2/3 complex inhibitor in plant cells. We hypothesized that applying CK-666 to wild-type Arabidopsis cells would inhibit the Arp2/3 complex activity and mimic the *arp2/3* mutant phenotypes described above. To test the effects of CK-666, we applied a dose series (0, 1, 5, 10, 50, and 100 μM) for 5 min and collected snapshots of epidermal cells from the apical region of treated hypocotyls. Compared to the mock treatment (0 μM), CK-666 started to have a significant reduction on both filament density and the extent of bundling at 5 μM and reached its maximum effect at 10–50 μM (Supplemental Figure S2, A–C). A time-course (0, 5, 10, 30, and 60 min) of 10 μM CK-666 treatment showed that 5 min was sufficient to alter actin array organization (Supplemental Figure S2, A, D, and E). Finally, cells were able to recover normal actin array architecture from a 5 min, 10 μM CK-666 application after a 30-min wash out (Supplemental Figure S2, A, F, and G).

To further examine whether CK-666 phenocopies *arp2/3* mutants, we treated 5-d-old dark-grown hypocotyls of wild type and *arp2-1* with either mock solution or 10 μM CK-666 for 5 min and measured actin organization and single filament dynamics. Compared to mock-treated wild-type cells, the CK-666-treated wild-type cells had significantly decreased filament abundance (Figure 5, A and B), extent of filament bundling (Figure 5, A and C), as well as overall nucleation frequency (Figure 3B), and these changes mirrored actin organization in mock-treated *arp2-1* cells. Moreover, treatment of *arp2-1* with CK-666 showed no differences in terms of filament organization or dynamics compared to *arp2-1* alone (Figure 5, A– D; Figure 3B). CK-666 treatment also potently suppressed side-branched filament nucleation in wild-type cells, but not end or *de novo* filament origins (Figure 3C; Supplemental Movies S1 and S8), thereby fully phenocopying the effects of *arp2-1*. Finally, treatment of *arp2-1* with CK-666 did not further reduce filament side-branch nucleation events, indicating that its likely mode of

action is to inhibit daughter filament formation from a mother filament by the Arp2/3 complex (Figure 3C; Supplemental Movies S8 and S9).

When we compared CK-666 treatment of *arpc2* with its wild-type siblings, there were similar changes in actin architecture and filament nucleation frequency (Supplemental Figure S1 and S3). Therefore, we validated CK-666 as a small molecule inhibitor that targets the Arp2/3 complex and demonstrate its utility as an acute but reversible inhibitor for studying the Arp2/3 complex in Arabidopsis.

The Arp2/3 complex and formins are both capable of nucleating side-branched filaments

Our previous work showed that profilin-bound actin monomers favor formin-mediated fast actin filament elongation at rates > 2 μm/s (Cao et al., 2016), and the data above suggest that Arp2/3-nucleated filament barbed ends elongated at intermediate rates of 1.25 – 1.5 μm/s (Figure 4B; Supplemental Figure S1E). We previously demonstrated the effectiveness of Small Molecule Inhibitor of Formin Homology 2 (SMIFH2) in Arabidopsis (Cao et al., 2016). Actin array organization and nucleation frequency were significantly reduced when wild-type cells were treated with 25 μM SMIFH2 for 5 min (Cao et al., 2016), and similar results were obtained here (Figure 6; Figure 7; Supplemental Movie S10).

To test whether filament arrays generated by these two nucleators are distinct, we genetically- and/or chemically-inhibited the Arp2/3 complex and formins. Both Arp2/3-inhibited (mock-treated *arp2-1* or *arpc2)* or formin-inhibited (SMIFH2-treated wild type) cells had a significant decrease in actin filament abundance compared to mock-treated wild type (Figure 6, A and B; Supplemental Figure S4, A and B). However, SMIFH2 treatment of wild type led to only a modest reduction in the extent of bundling (Figure 6, A and C; Supplemental Figure S4, A and C), whereas *arp2/3* mutants had a substantial reduction in bundling. Moreover, filaments were more parallel to each other when the Arp2/3 complex was inhibited compared to the ones with formin activity suppressed (Figure 6D; Supplemental Figure S4D). Thus, both the Arp2/3 complex and formins are required to generate dense arrays of individual actin filaments, however, their contributions to actin filament bundling and parallelness are distinct.

To test whether filament dynamics or types and extent of filament nucleation are distinctly due to the Arp2/3 complex or formins, we examined single filament dynamics in genetically- and/or chemically- inhibited material. The nucleation frequency of both total and side-branching filaments was significantly decreased in both Arp2/3-inhibited (mock-treated

arp2-1) and formin-inhibited (SMIFH2-treated wild type) cells compared to wild type (Figure 7A; Supplemental Movies S2 and S10), and the nucleation frequency of side-branched filaments in Arp2/3-inhibited cells (0.082 ± 0.022 events/filament/min) was ~50% less than in formin-inhibited cells (0.16 ± 0.013 events/filament/min). However, the nucleation frequency due to *de novo* filament origins was not influenced when either the Arp2/3 complex or formin were suppressed (Figure 7A). The average filament elongation rate in Arp2/3-inhibited cells (1.85 ± 0.10 μm/s) was also significantly higher than the rate in formin-inhibited cells (1.57 ± 0.11 μm/s) or in wild-type cells (1.72 ± 0.10 μm/s). In addition, the population distribution of filament elongation rates in Arp2/3-inhibited cells was significantly left-skewed (peak value at 2.0 – 2.25 μm/s) compared to wild type (peak value at 1.25 – 1.5 μm/s), whereas formin-inhibited cells lost a large portion of filaments elongating at 2.0 – 2.25 μm/s but the distribution had a prominent peak at 1.0 – 1.5 μm/s (Figure 7E). We did not, however, observe any significant difference in filament length, lifetime, or filament severing frequency when parameters of side-branched filaments in Arp2/3-inhibited cells and formin-inhibited cells were compared (Figure 7, B–D). Again, we found similar results in both actin architecture (Supplemental Figure S4) and single filament dynamics (Supplemental Figure S5) when *arpc2* and its respective wild-type line treated with mock solution or SMIFH2 were compared. These data indicated that both the Arp2/3 complex and formin predominantly generate side-branched actin filaments and formin-nucleated filaments elongate faster than Arp2/3-nucleated ones.

To test whether SMIFH2 has off-target inhibition of myosin superfamily members as reported in Drosophila (Nishimura et al., 2021), we evaluated the influence of SMIFH2 (and CK-666) on the activity of myosin XIK, the major myosin isoform mediating the delivery, vesicle tethering, and exocytosis of secretory vesicles in Arabidopsis cells (Zhang et al., 2021). We found that neither SMIFH2 or CK-666 treatment reduced the speed of myosin XIK-YFP motility compared to pentabromopseudilin (PBP), an effective myosin inhibitor in plant cells (Supplemental Figure S6, B–D) (Zhang et al., 2019). In addition, we also measured the filament convolutedness and the rate of change of convolutedness of actin filaments, which are parameters describing the buckling and straightening of filaments (Staiger et al., 2009; Cai et al., 2014). Both parameters were significantly decreased with SMIFH2 and PBP treatment, but unchanged by CK-666, indicating that SMIFH2 does indeed alter filament buckling and straightening (Supplemental Table S2; Supplemental Figure S6A). These data suggest that SMIFH2 may not have an off-target effect on activities of myosin based on the lack of effect on the motility of YFP-XIK, but it is still possible that SMIFH2 targets other myosin isoforms besides

myosin XIK. Although the inhibition of filament buckling and straightening could indicate an off-target effect of SMIFH2 on myosin XI, it seems equally likely that filament buckling is caused by the processive assembly of actin filaments by Arabidopsis formins (Supplemental Table S2).

Combined genetic and chemical inhibition of Arp2/3 and formins increases spontaneous filament nucleation and overall actin filament abundance

Using chemical and genetic tools to suppress the activity of both the Arp2/3 complex and formin simultaneously, we applied SMIFH2 to *arp2-1 or arpc2* cells, or treated wild-type cells with a combination of SMIFH2 and CK-666, to test whether different nucleators cooperate or compete to form actin filament arrays in plant cells. Since the Arp2/3 complex and formin are, so far, the only two actin filament nucleators identified in plant cells, we predicted that inhibiting both the Arp2/3 complex and formin should severely suppress actin filament nucleation activities and significantly reduce filament abundance. Surprisingly, in *arp2-1* cells treated with SMIFH2, actin filament abundance was dramatically increased compared to cells with normal Arp2/3 complex and formin activities or with only one nucleator inhibited (Figure 6, A and B). Notably, SMIFH2-treated *arp2-1* cells had a marked abundance of short, single actin filaments in the cortical array (Figure 6A). Unlike actin array density, the extent of actin filament bundling was not restored to wild-type levels when both the Arp2/3 complex and formins were inhibited; indeed, overall bundling was lower in SMIFH2-treated *arp2-1* compared to *arp2-1* alone (Figure 6, A and C). In addition to increased filament abundance, total filament nucleation frequency was significantly increased when both the Arp2/3 complex and formin activities were reduced, and a 2.5-fold enhancement of *de novo* filament origins was responsible for this increase (Figure 7A; Supplemental Movie S11). However, the lengths of filaments generated *de novo* or from the side-branching nucleation events were both significantly reduced in SMIFH2-treated *arp2-1* cells compared to other treatments and genotypes (Figure 7B). Finally, we also observed similar phenotypes in both actin architecture and filament dynamics when we applied SMIFH2 to *arpc2* (Supplemental Figure S5) or applied both CK-666 and SMIFH2 to wild type (Figure 8). These results indicate that a marked increase in *de novo* filament nucleation results when both the Arp2/3 complex and formins are inhibited in plant cells.

Discussion

In this study, we utilized a combination of genetic mutations or small molecule inhibitors along with high spatiotemporal resolution fluorescence microscopy to demonstrate, for the first time, that the Arp2/3 complex nucleates side-branched actin filaments in Arabidopsis epidermal cells. We found that the Arp2/3 complex mutants, *arp2-1* and *arpc2*, had a dramatically reduced overall abundance of actin filaments in the cortical array, a reduction in the extent of filament bundles, and a significantly decreased frequency of side-branched nucleation events. In addition, acute treatment of wild-type plants with CK-666 phenocopied the actin-based defects observed in *arp2/3* mutants, whereas applying CK-666 to *arp2/3* mutants did not have any additional effect on overall actin structure or filament dynamics. Thus, we confirmed that these actin-based defects correlated with the loss of functional Arp2/3 complex and also established that CK-666 is an effective tool for inhibition of the Arp2/3 complex in plant cells. Through experiments comparing genetic and chemical inhibition of the Arp2/3 complex or formins, we observed that both proteins were capable of nucleating side-branched actin filaments, but that Arp2/3-nucleated filaments grew slower and were shorter than formin-nucleated ones. Surprisingly, simultaneous inhibition of both the Arp2/3 complex and formins led to an increase in actin filament abundance and dramatically promoted *de novo* nucleation events. These observations indicate that the regulatory mechanisms for actin filament nucleation in the homeostatic cortical array of plant cells are different from yeast or animal cells.

The Arp2/3 complex is a major nucleator of side-branched actin filaments in *Arabidopsis* epidermal cells

Nucleation is the rate-limiting step for actin filament formation in vitro and depends on the availability of actin monomers and is suppressed by profilin (Pollard et al., 2000; Sept and McCammon, 2001; Michelot et al., 2005). In cells, filament nucleation is also accepted as a key step in generating new actin arrays for various cellular activities, such as driving animal cell migration and powering organelle movements. Biochemical studies demonstrate that the Arp2/3 complex and formins use different molecular mechanisms to overcome the rate-limiting step for filament formation and they typically create different types of actin structure. After creating a nucleus, representing the first three subunits of a two-stranded helix, and initiating filament elongation, the Arp2/3 complex remains attached at the nucleation site and the filament barbed

end is free for the addition of actin monomers, profilin-actin, or capping protein (Mullins et al., 1998; Amann and Pollard, 2001; Fujiwara et al., 2002; Ichetovkin et al., 2002; Rouiller et al., 2008). In contrast, formins overcome the suppression of nucleus formation by directly interacting with profilin and actin through FH1 and FH2 domains. After the nucleation step, many formins remain associated at the barbed end of actin filaments and processively facilitate filament elongation through the addition of profilin-actin. This allows formin-associated filaments to grow much faster and longer compared to filaments with free barbed ends that are typically bound by heterodimeric capping protein (CP) soon after initiation. The occupation of formin at the barbed end can also prevent CP from binding and limiting subunit addition or loss (Kovar and Pollard, 2004; Romero et al., 2004; Kovar, 2006). Based on these observations, the conventional model of actin nucleation posits that formins generate long, unbranched filaments with a fast filament elongation rate whereas the Arp2/3 complex nucleates short, branched actin networks with a slower growth rate.

The Arp2/3 complex has been accepted as the major nucleator of side-branched actin filaments in yeast and animal cells (Mullins et al., 1998; Amann and Pollard, 2001; Fujiwara et al., 2002; Ichetovkin et al., 2002; Rouiller et al., 2008). Even though the Arp2/3 complex is also shown to be critical for plant cells to maintain their homeostatic actin organization and is required for epidermal cell morphogenesis, defense against fungal penetration, auxin transportation, and other cellular activities, little is known about the exact function of plant Arp2/3 complex in terms of its contribution in regulating actin filament dynamics. In this study, we characterized the function of the Arp2/3 complex in regulating the organization of the cortical actin array as well as single actin filament dynamics in living Arabidopsis cells. Epidermal cells of dark-grown hypocotyls with genetically- or chemically-inhibited Arp2/3 complex showed a quantifiable decrease in both actin filament abundance and extent of filament bundling, and, more importantly, there was a significantly reduced nucleation frequency of side-branched actin filaments. Branched filament formation represents more than half of all nucleation events in the cortical actin array of hypocotyl epidermal cells and these are reduced by 60–70% when the Arp2/3 complex was inhibited chemically or genetically. These results suggest that the Arp2/3 complex is a major nucleator of side-branched actin filaments in Arabidopsis epidermal cells. Our data also provide the first live cell view of the formation of branched actin filaments by active Arp2/3 complex at single filament resolution. Furthermore, our results reveal that there are at least two populations of filaments with different dynamic properties, likely due to different filament growth mechanisms and/or availability of filament barbed ends for monomer addition,

that contribute to the organization of the homeostatic actin cortical array in epidermal cells. By examining filament elongation rate frequencies when formin activity was suppressed, or when both the Arp2/3 complex and formins were inhibited, filaments with elongation rates of 1 – 1.25 µm/s predominated. We expect this represents the population of filaments with free barbed ends extending by monomer addition and is consistent with the in vitro mechanism of branched filament nucleation by the Arp2/3 complex.

The Arp2/3 complex and formins both mediate side-branched filament nucleation but generate filaments with unique dynamic properties

Previous results with the fission and budding yeasts, *Schizosaccharomyces pombe* and *Saccharomyces cerevisiae*, as well as mammalian cells reveal a competition between the Arp2/3 complex and formin for a limited pool of actin monomers; consequently, formin-mediated long filament bundles dominate when the Arp2/3 complex is inhibited, whereas an increased abundance of actin patches created by the Arp2/3 complex are prominent when formin is down-regulated (Hotulainen and Lappalainen, 2006; Burke et al., 2014; Lomakin et al., 2015; Suarez et al., 2015; Fritzsche et al., 2016; Davidson et al., 2018; Antkowiak et al., 2019; Chan et al., 2019; Kadzik et al., 2020). Plant cells, by contrast, appear to show cooperation between these two nucleators rather than a competition to build distinct actin arrays. The cortical cytoplasm of epidermal cells contains a dynamic actin array that is rather disordered and comprises comingled actin filament bundles and individual actin filaments (Staiger et al., 2009; Smertenko et al., 2010). Evidence for actin patches or dense dendritic actin networks is limited to certain cell types, such as guard mother cells (Facette et al., 2015), the apex of trichomes (Yanagisawa et al., 2015), or at focal sites elicited by pathogen attack (Hardham et al., 2007; Qin et al., 2021). Our results revealed that the density of actin filaments in the cortical array, extent of filament bundling, as well as filament nucleation frequency all decreased when either the Arp2/3 complex or formins were inhibited, suggesting that formins were not able to maintain the actin abundance at normal levels when the Arp2/3 complex was genetically or chemically inhibited, and the Arp2/3 complex also failed to do so when formins were inhibited. These results indicate that plant cells may have a different actin regulatory mechanism for constructing actin filament arrays compared to yeast or some animal cells. Our results are consistent with a previous report showing partial cooperation between plant filament nucleation mechanisms in Arabidopsis cotyledon epidermal cells, but the consequences of losing either class of nucleator were markedly different (Cifrová et al., 2020). That study showed a minor increase in actin filament

density in either the formin *fh1* mutant or the *arpc5* mutant (Cifrová et al., 2020), rather than the prominent decreases observed here. These differences could be due to the use of different actin filament reporters (LifeAct versus fABD2), different developmental state and organ for examining epidermal cells (cotyledons versus dark-grown hypocotyls), or the result of compensation from genetic loss of one formin isoform versus acute treatment with a chemical inhibitor. The previous results are also not obviously consistent with the loss of nucleation machinery; however, individual filament dynamics were not examined to test whether nucleation activity or filament formation was suppressed by the loss of the Arp2/3 complex or AFH1.

Our results showed that both the Arp2/3 complex and formins are responsible for generating side-branched filaments because the inhibition of either one led to a significant reduction in side-branched filament nucleation and did not promote the other two types of filament nucleation. These results also suggest that the Arp2/3 complex and formins are not competing for actin monomers for filament nucleation. Based on the total actin concentration and the ratio of F-actin to total actin in both maize pollen and poppy pollen, the estimated actin monomer pool in Arabidopsis hypocotyl cells is relatively large and most monomers are likely to be in a profilin-actin complex (Staiger et al., 2010); therefore, the Arp2/3 complex and formins may not have to compete for a limited supply of actin monomers in plant cells. Here, if we assume that 1.25 μm/s is the rate of addition of monomers to free barbed ends, that the association rate constant for plant actin is similar to ATP-loaded rabbit skeletal muscle α-actin ($k_+ = 11.6\ \mu M^{-1}\ s^{-1}$) and that a micron of actin filament comprises 370 subunits (Pollard et al., 2000), then we estimate the available monomer pool to be 40 μM in hypocotyl epidermal cells using the equation: [G-actin] = rate/k_+. In addition, even though both the Arp2/3 complex and formins generate side-branched actin filaments, these filaments have markedly different properties. We found that formin-nucleated filaments grew significantly faster at rates of 2 – 2.25 μm/s, with another small subpopulation growing at rates > 3 μm/s. The different properties of filament barbed ends as well as a large pool of monomers perhaps buffered with profilin may facilitate the fast-growing filaments nucleated by side-branching as previously found in Arabidopsis cells (Cao et al., 2016), and is consistent with previous in vitro results (Vavylonis et al., 2006; Michelot et al., 2013; Suarez et al., 2015; Funk et al., 2019).

If using the conventional model for how formins generate new actin filaments, we should expect that plant processive formins not only generate growing filaments from the side of a mother filament but also remain attached to the barbed end of the new filament to facilitate the

addition of profilin-actin to the growing ends, which results in faster and longer side-branched filaments compared to Arp2/3-nucleated ones. However, previous in vitro data showed that the formin AFH1 nucleates actin filaments but remains associated at the pointed end and does not compete with capping protein for filament barbed ends, indicating it is non-processive and associates with the side of filaments after nucleation (Michelot et al., 2006). Further, SMIFH2 application in our studies reduced nucleation frequency but did not reduce the filament length of side-branched filaments compared to the mock treatment. Both in vitro and in vivo results suggest that non-processive formins in plant cells may have a weak interaction with filament barbed ends so that these formins move away from the end of the filament to its side to generate a new side-branched filament instead of occupying the barbed end and facilitating filament elongation. However, another in vitro analysis showed that the processive formin, AtFH14, promotes *de novo* filament growth via the association with profilin (Zhang et al., 2016), and there are 21 FORMIN homologs in *Arabidopsis* (Cvrčková et al., 2004; Blanchoin and Michelot, 2012; Cvrčková, 2013). All these results suggest that plant formins that nucleate side-branched filaments may have distinct molecular properties to formins that nucleate *de novo* filament formation or formins found in yeast or animal cells. It is important to note that SMIFH2 is capable of suppressing the nucleation activity of the non-processive AFH1 in vitro (Cao et al., 2016), so it seems probable that at least one class of plant formins is being suppressed in inhibitor-treated cells.

Since SMIFH2 shows off-target inhibition of members of the myosin superfamily (Nishimura et al., 2021), we are compelled to critically evaluate the effects of SMIFH2 treatment on plant cells. Although our data showed that SMIFH2 treatment did not influence the motility of myosin XIK, it did significantly reduce filament convolutedness and the rate of change of convolutedness of actin filaments, suggesting that SMIFH2 alters filament buckling and straightening. However, the change in filament buckling could be the consequence of different filament growth rates and processive elongation by formins (Staiger et al., 2009; Cai et al., 2014; Cao et al., 2016). Even though a recent in vitro study reveals that SMIFH2 is a pan-inhibitor for all human formins (Orman et al., 2022), we should not exclude the possibility that SMIFH2 can only inhibit a subset of plant formin homologs. These facts suggest that we need to be cautious about making conclusions concerning formin in vivo functions since this conclusion relies solely on SMIFH2 inhibition. Further genetic and biochemical analyses should be designed to dissect the interaction between SMIFH2 and different formin homologs in order to determine the specificity of this chemical inhibitor on plant formins.

Simultaneous inhibition of the Arp2/3 complex and formins promotes *de novo* nucleation events

When we combined genetic and chemical methods to downregulate the Arp2/3 complex and formins simultaneously, surprisingly, the frequency of actin filament nucleation was significantly enhanced, with *de novo* nucleation events appearing to be the exclusive contributor to this enhancement. A relevant experiment in Arabidopsis cotyledon epidermal pavement cells with the *fh1 arpc5* double mutant also showed a minor increase in actin density, however filament nucleation was not measured (Cifrová et al., 2020). The Arp2/3 complex and formins are, to date, the only two *bona fide* actin filament nucleators in plant cells (Blanchoin and Staiger, 2010; Vaškovičová et al., 2013; Yanagisawa et al., 2013). Theoretically, when both the Arp2/3 complex and formins are inhibited, the concentration of free actin monomers is predicted to increase but the ratio of F- to G-actin and the proportion of profilin-actin in the monomer pool should both decrease. It is possible that these changes in the actin monomer pool could increase the nucleation rate of spontaneous filament formation thereby enhancing the total frequency of *de novo* nucleation events. In support of this model, disruption of AtPRF1 led to an increase in *de novo* nucleation events and a decrease in side-branched events (Cao et al., 2016). Here, the amount of *de novo* filaments was dramatically increased when both the Arp2/3 complex and formins were inhibited but the average length was significantly shorter compared to the ones generated from other origins. This observation fits the previous biochemical study that showed the relationship between the average length of filaments grown *de novo* and the number of these filaments fits an exponential distribution instead of a Gaussian distribution (Burlacu and Borejdo, 1992).

A previous study with fission yeast reveals that inhibiting the Arp2/3 complex with CK-666 in a formin double mutant (*cdc12-112 for3⊿*) depletes most of the actin bundles but not the actin patches (Burke et al., 2014). The resulting actin arrays were rather static, however, unlike the dynamic arrays observed after simultaneous inhibition of the Arp2/3 complex and formins found in Arabidopsis cells. Another study with animal cells shows that although both classes of nucleator contribute to formation and dynamics of the cortical actin array, simultaneous inhibition of both nucleators results in a significant change in cortical actin abundance and structure that leads to a 50% reduction of cortical elasticity (Fritzsche et al., 2016). The different actin dynamic behaviors between yeast, animal and plant cells when both the Arp2/3 complex and formins are inhibited suggests a possible unique filament nucleation mechanism in plant cells that can overcome the requirement for these two major nucleators. However, considering

the fact that SMIFH2 treatment only inhibits the side-branched filament nucleation in Arabidopsis, we cannot rule out the possibility that our double inhibition treatment inhibited only a subclass of formins responsible for side-branch formation. In this case, the *de novo* filament nucleation by SMIFH2-insensitive formin homologs might become significantly enhanced. In addition, it is also possible that there is an unknown actin nucleator in Arabidopsis that facilitates *de novo* filament nucleation when the major side-branched filament nucleators are inhibited. This unknown nucleator may be inactive when the Arp2/3 complex and formins are present, or it may have a much lower binding affinity for actin monomers compared to the Arp2/3 complex and formins.

Another unexpected result from inhibiting the Arp2/3 complex or formins is that the extent of actin filament bundling decreased when either nucleator was downregulated, suggesting that side-branched actin filaments generated by both the Arp2/3 complex and formins are assembled into actin bundles. In addition, the downregulation of the Arp2/3 complex has a greater effect on the extent of filament bundling compared to formin inhibition, which may indicate that filaments generated by the Arp2/3 complex contribute more to the construction of actin bundles than the ones generated by formins.

In conclusion, our results provide direct evidence to demonstrate that the Arp2/3 complex nucleates side-branched actin filaments in living plant cells. These studies also confirm that some formin homologs generate side-branched actin filaments in plant cells, which is a unique actin filament nucleation mechanism compared to yeast or animal cells. Moreover, we find that Arp2/3- and formin-nucleated filaments have distinct dynamic properties, which can be applied to future studies about how cells coordinate these two nucleators to regulate the actin structure and dynamics for different cellular activities. The dual-inhibition of both the Arp2/3 complex and formin surprisingly caused an enhanced *de novo* filament nucleation, which raises the possibility for a unique actin nucleation mechanism to generate dynamic cortical actin arrays in plant cells.

Material and Methods

Plant Material and Growth Conditions

All Arabidopsis (*Arabidopsis thaliana*) plants in this study were in Columbia-0 (Col-0) background. The *ARP2* T-DNA insertion line, *arp2-1* (SALK_003448), was obtained from the Arabidopsis Biological Resource Center (Ohio State University) and the *ARPC2* point mutation line, *arpc2* (G1217A), was kindly provided by Dan Szymanski (Purdue University). Both *arp2-1* and *arpc2* mutant lines were crossed to wild-type (Col-0) expressing the GFP-fABD2 reporter (Sheahan et al., 2004; Staiger et al., 2009) and homozygous mutants and corresponding wild-type siblings were recovered from F2 populations.

Seeds were surface sterilized and stratified at 4°C for 3 days on plates comprising half-strength Murashige and Skoog (MS) medium supplemented with 1% (w/v) sucrose and 1% (w/v) agar. For dark-grown hypocotyl growth, seedlings were grown in continuous darkness after exposing the plates to light for 4 h. For light-grown root growth, seeds were grown vertically on plates comprising half-strength MS medium supplemented with 0% (w/v) sucrose and 0.6% (w/v) agar under long-day conditions (16 h light/8h dark) at 21°C.

A double-blinded experimental design was used for all phenotypic analyses. All image measurements were performed with Image J (National Institutes of Health, Bethesda, MD. http://rsb.info.nih. gov/ij/).

Drug Treatments

For short-term live cell treatments, individual seedlings were treated for 5 min in inhibitor solution in 6-well plates in the dark prior to each imaging session. Hypocotyls were mounted in the inhibitor solution and imaged immediately. CK-666 (Sigma-Aldrich; Cat # 182515; St. Louis, MO, USA) and SMIFH2 (Sigma-Aldrich; Cat # 344092) were dissolved in DMSO to prepare a 5 mM stock solution.

Live Cell Imaging

For both snapshot and time-lapse image acquisitions, epidermal cells from the apical region of 5-d-old dark-grown hypocotyls were used unless otherwise stated. In some experiments, the lipophilic dye, FM4-64 (Invitrogen; Cat # T3166; Carlsbad, CA, USA), was dissolved in DMSO

and used at 20 mM to label the plasma membrane. All images and movies were collected using variable-angle epifluorescence microscopy (VAEM) with an Olympus TIRF objective (60X, 1.45 numerical aperture) as described previously (Staiger et al., 2009; Henty et al., 2011; Li et al., 2012; Cai et al., 2014; Cao et al., 2016).

For actin architecture analysis, more than 200 images of hypocotyl epidermal cells were collected from at least 15 individual seedlings per genotype or drug treatment. For single actin filament dynamics analysis, more than 50 filaments from at least 10 hypocotyls were measured per genotype or drug treatment. For nucleation frequency analysis, more than 300 events from 10 hypocotyls were observed per genotype or drug treatment. All experiments were conducted with at least 3 biological repeats and one representative dataset is shown in each figure.

Image Processing and Quantitative Analysis of Actin Cytoskeleton Architecture and Single Actin Filament Dynamics

Images and movies were acquired using SlideBook software (version 5.5; Intelligent Imaging Innovations) and processed with Image J (Adobe Systems). All images used for actin architecture analysis were collected with a fixed exposure time, laser power, and camera gain setting.

To quantify actin architecture, four parameters, *density*, *skewness*, *angle*, and *parallelness*, were employed in this study; density and skewness measure the percentage of occupancy of GFP signal in an image and the extent of actin filament bundling respectively, angle and parallelness describe how filaments orient relative to the longitudinal axel of the cell or each other respectively (Higaki et al., 2010; Ueda et al., 2010; Henty et al., 2011; Li et al., 2012; Cai et al., 2014; Cao et al., 2016; Arieti and Staiger, 2020). Micrographs were analyzed in Image J using the methods described previously (Higaki et al., 2010; Henty et al., 2011; Li et al., 2012).

To compare single actin filament parameters between genotype or drug treatment, double-blind experiments (data collection and analysis) were performed. Maximum filament length and lifetime, filament severing frequency, elongation rates, filament convolutedness and the rate of change of convolutedness were measured as described previously (Staiger et al., 2009; Henty et al., 2011; Li et al., 2012; Cai et al., 2014; Cao et al., 2016). For nucleation frequency analysis, a 400 μm^2 ROI was randomly selected from movies of epidermal cells at the

apical region of the hypocotyl, and all observable nucleation events were counted during a time period of 100 s, according to Cao et al., 2016. To account for differences in filament density in genotypes or drug treatments, the nucleation frequency was normalized against filament numbers in each ROI.

Statistical Analysis

One-way ANOVA with Tukey's post-hoc tests were performed in SPSS (version 25) to determine the significance among different treatments. Two-tailed Student's t test was performed in Excel 15.32. Any difference with a P value over 0.05 was considered significantly different.

Supplemental Online Data

Table S1. Single actin filament dynamics in wild type (*ARPC*2) and *arpc2* mutant with or without CK-666.
Table S2. Actin filament shape dynamics in mock- and inhibitor-treated wild-type (Col-0) epidermal cells.
Figure S1. Actin filament nucleation frequency is decreased in *arpc2* and after treatment of wild type with CK-666.
Figure S2. CK-666 is an acute and reversible chemical inhibitor of the Arp2/3 complex in plant cells.
Figure S3. Actin architecture is perturbed in *arpc2* and the reduced filament density and bundling phenotypes are recapitulated by treatment with CK-666.
Figure S4. Actin filament density increases after treatment of *arpc2* with the formin inhibitor SMIFH2.
Figure S5. Overall filament nucleation and *de novo* filament formation increase when ARPC2 and formin activity are simultaneously inhibited.
Figure S6. Filament convolutedness decreases when formin or myosin activities are inhibited.

Movie S1. Full time-lapse sequence of actin filament nucleation activities in mock-treated wild-type (*ARP2*) cells.
Movie S2. Full time-lapse sequence of actin filament nucleation activities in mock-treated *arp2-1* cells.
Movie S3. Representative actin filament nucleated *de novo* from the cytoplasm (as in Figure 3 A, top row).
Movie S4. Representative actin filament nucleated from the side of a pre-existing filament (as in Figure 3 A, middle row).
Movie S5. Representative actin filament nucleated from the end of a pre-existing filament (as in Figure 3 A, bottom row).
Movie S6. Representative example of filament elongation (as in Figure 4 A).
Movie S7. Representative example of filament severing (as in Figure 4 A).
Movie S8. Full time-lapse sequence of actin filament nucleation activities in CK-666-treated wild-type (*ARP2*) cells.
Movie S9. Full time-lapse sequence of actin filament nucleation activities in CK-666-treated *arp2-1* cells.
Movie S10. Full time-lapse sequence of actin filament nucleation activities in SMIFH2-treated wild-type (*ARP2*) cells.
Movie S11. Full time-lapse sequence of actin filament nucleation activities in SMIFH2-treated *arp2-1* cells.

Acknowledgments

We thank Hongbing Luo (Purdue University) for excellent care and maintenance of plant materials, Dan Szymanski (Purdue University) for providing the *arpc2* line, and David Kovar (University of Chicago) and Laurent Blanchoin (Interdisciplinary Research Institute of Grenoble) for helpful comments on the manuscript. We are also grateful to the Arabidopsis Biological Resource Center (Ohio State University) for supplying the *arp2-1* T-DNA insertion line. The TIRF microscopy facility was supported, in part, by the Bindley Bioscience Center at Purdue University. This work was funded by a grant from the Physical Biosciences program of the US Department of Energy, Office of Basic Energy Sciences (DE-FG02-09ER15526) to C.J.S. Conceptualization of experiments and manuscript preparation by C.J.S. were supported by the EMBRIO Institute, an NSF-Biological Integration Institute under contract no. 2120200.

The authors declare no competing financial interests.

Author Contributions

L. Xu acquired and analyzed data, prepared figures, wrote and revised the manuscript; L. Cao acquired and analyzed data; J. Li acquired and analyzed data; C.J. Staiger conceptualized experiments, acquired funding, wrote and revised the manuscript.

References

Akin, O., and Mullins, R.D. (2008). Capping protein increases the rate of actin-based motility by promoting filament nucleation by the Arp2/3 complex. Cell **133,** 841-851.

Ali, M.F., Fatema, U., Peng, X., Hacker, S.W., Maruyama, D., Sun, M.-X., and Kawashima, T. (2020). ARP2/3-independent WAVE/SCAR pathway and class XI myosin control sperm nuclear migration in flowering plants. Proc. Natl. Acad. Sci. USA **117,** 32757-32763.

Amann, K.J., and Pollard, T.D. (2001). Direct real-time observation of actin filament branching mediated by Arp2/3 complex using total internal reflection fluorescence microscopy. Proc. Natl. Acad. Sci. USA **98,** 15009-15013.

Antkowiak, A., Guillotin, A., Boiero Sanders, M., Colombo, J., Vincentelli, R., and Michelot, A. (2019). Sizes of actin networks sharing a common environment are determined by the relative rates of assembly. PLoS Biol. **17,** e3000317.

Arieti, R.S., and Staiger, C.J. (2020). Auxin-induced actin cytoskeleton rearrangements require AUX1. New Phytol. **226,** 441-459.

Beltzner, C.C., and Pollard, T.D. (2008). Pathway of actin filament branch formation by Arp2/3 complex. J. Biol. Chem. **283,** 7135-7144.

Blanchoin, L., and Staiger, C.J. (2010). Plant formins: Diverse isoforms and unique molecular mechanism. Biochim. Biophys. Acta **1803,** 201-206.

Blanchoin, L., and Michelot, A. (2012). Actin cytoskeleton: a team effort during actin assembly. Curr. Biol. **22,** R643-R645.

Burke, T.A., Christensen, J.R., Barone, E., Suarez, C., Sirotkin, V., and Kovar, D.R. (2014). Homeostatic actin cytoskeleton networks are regulated by assembly factor competition for monomers. Curr. Biol. **24,** 579-585.

Burlacu, S., and Borejdo, J. (1992). Motion of actin filaments in the presence of myosin heads and ATP. Biophys. J. **63,** 1471-1482.

Cabrera, R., Suo, J., Young, E., and Chang, E.C. (2011). *Schizosaccharomyces pombe* Arc3 is a conserved subunit of the Arp2/3 complex required for polarity, actin organization, and endocytosis. Yeast **28,** 495-503.

Cai, C., Henty-Ridilla, J.L., Szymanski, D.B., and Staiger, C.J. (2014). Arabidopsis myosin XI: a motor rules the tracks. Plant Physiol. **166,** 1359-1370.

Cao, L., Henty-Ridilla, J.L., Blanchoin, L., and Staiger, C.J. (2016). Profilin-dependent nucleation and assembly of actin filaments controls cell elongation in Arabidopsis. Plant Physiol. **170,** 220-233.

Carlier, M.-F., and Shekhar, S. (2017). Global treadmilling coordinates actin turnover and controls the size of actin networks. Nat. Rev. Mol. Cell Biol. **18,** 389-401.

Chan, F.Y., Silva, A.M., Saramago, J., Pereira-Sousa, J., Brighton, H.E., Pereira, M., Oegema, K., Gassmann, R., and Carvalho, A.X. (2019). The ARP2/3 complex prevents excessive formin activity during cytokinesis. Mol. Biol. Cell **30,** 96-107.

Cheung, A.Y., and Wu, H.-m. (2004). Overexpression of an Arabidopsis formin stimulates supernumerary actin cable formation from pollen tube cell membrane. Plant Cell **16,** 257-269.

Cifrová, P., Oulehlová, D., Kollárová, E., Martinek, J., Rosero, A., Žárský, V., Schwarzerová, K., and Cvrčková, F. (2020). Division of labor between two actin nucleators-the formin FH1 and the ARP2/3 complex-in *Arabidopsis* epidermal cell morphogenesis. Front. Plant Sci. **11,** 148.

Cvrčková, F. (2013). Formins and membranes: anchoring cortical actin to the cell wall and beyond. Front. Plant Sci. **4,** 436.

Cvrčková, F., Bavlnka, B., and Žárský, V. (2000). Identification and cloning of AtFORMIN1, an *Arabidopsis thaliana* formin homologue. Biochem. Soc. Trans. **28,** A208-A208.

Cvrčková, F., Novotný, M., Pícková, D., and Žárský, V. (2004). Formin homology 2 domains occur in multiple contexts in angiosperms. BMC Genomics **5,** 44.

Davidson, A.J., Amato, C., Thomason, P.A., and Insall, R.H. (2018). WASP family proteins and formins compete in pseudopod- and bleb-based migration. J. Cell Biol. **217,** 701-714.

Dayel, M.J., and Mullins, R.D. (2004). Activation of Arp2/3 complex: addition of the first subunit of the new filament by a WASP protein triggers rapid ATP hydrolysis on Arp2. PLoS Biol. **2,** 476-485.

Deeks, M.J., Hussey, P.J., and Davies, B. (2002). Formins: intermediates in signal-transduction cascades that affect cytoskeletal reorganization. Trends Plant Sci. **7,** 492-498.

El-Assal, S.E.-D., Le, J., Basu, D., Mallery, E.L., and Szymanski, D.B. (2004). DISTORTED2 encodes an ARPC2 subunit of the putative *Arabidopsis* ARP2/3 complex. Plant J. **38,** 526-538.

Facette, M.R., Park, Y., Sutimantanapi, D., Luo, A., Cartwright, H.N., Yang, B., Bennett, E.J., Sylvester, A.W., and Smith, L.G. (2015). The SCAR/WAVE complex polarizes PAN receptors and promotes division asymmetry in maize. Nat. Plants **1,** 14024.

Fritzsche, M., Erlenkamper, C., Moeendarbary, E., Charras, G., and Kruse, K. (2016). Actin kinetics shapes cortical network structure and mechanics. Sci Adv **2,** e1501337.

Fujiwara, I., Suetsugu, S., Uemura, S., Takenawa, T., and Ishiwata, S. (2002). Visualization and force measurement of branching by Arp2/3 complex and N-WASP in actin filament. Biochem. Biophys. Res. Commun. **293,** 1550-1555.

Funk, J., Merino, F., Venkova, L., Heydenreich, L., Kierfeld, J., Vargas, P., Raunser, S., Piel, M., and Bieling, P. (2019). Profilin and formin constitute a pacemaker system for robust actin filament growth. eLife **8**.

Gao, X.-Q., Wang, X.-L., Ren, F., Chen, J., and Wang, X.-C. (2009). Dynamics of vacuoles and actin filaments in guard cells and their roles in stomatal movement. Plant, Cell & Environment **32,** 1108-1116.

García-González, J., Kebrlová, S.t.p.n., Semerák, M., Lacek, J., Kotannal Baby, I., Petrášek, J., and Schwarzerová, K. (2020). Arp2/3 Complex Is Required for Auxin-Driven Cell Expansion Through Regulation of Auxin Transporter Homeostasis. Front. Plant Sci. **11,** 486.

Hardham, A.R., Jones, D.A., and Takemoto, D. (2007). Cytoskeleton and cell wall function in penetration resistance. Curr. Opin. Plant Biol. **10,** 342-348.

Harries, P.A., Pan, A., and Quatrano, R.S. (2005). Actin-related protein2/3 complex component ARPC1 is required for proper cell morphogenesis and polarized cell growth in *Physcomitrella patens*. Plant Cell **17,** 2327-2339.

Henty, J.L., Bledsoe, S.W., Khurana, P., Meagher, R.B., Day, B., Blanchoin, L., and Staiger, C.J. (2011). *Arabidopsis* actin depolymerizing factor4 modulates the stochastic dynamic behavior of actin filaments in the cortical array of epidermal cells. Plant Cell **23,** 3711-3726.

Henty-Ridilla, J.L., Li, J., Blanchoin, L., and Staiger, C.J. (2013a). Actin dynamics in the cortical array of plant cells. Curr. Opin. Plant Biol. **16,** 678-687.

Henty-Ridilla, J.L., Shimono, M., Li, J., Chang, J.H., Day, B., and Staiger, C.J. (2013b). The plant actin cytoskeleton responds to signals from microbe-associated molecular patterns. PLoS Pathog. **9,** e1003290.

Hetrick, B., Han, M.S., Helgeson, L.A., and Nolen, B.J. (2013). Small molecules CK-666 and CK-869 inhibit actin-related protein 2/3 complex by blocking an activating conformational change. Chem. Biol. **20,** 701-712.

Higaki, T., Kutsuna, N., Sano, T., Kondo, N., and Hasezawa, S. (2010). Quantification and cluster analysis of actin cytoskeletal structures in plant cells: role of actin bundling in stomatal movement during diurnal cycles in Arabidopsis guard cells. Plant J. **61,** 156-165.

Hotulainen, P., and Lappalainen, P. (2006). Stress fibers are generated by two distinct actin assembly mechanisms in motile cells. the Journal of Cell Biology **173,** 383-394.

Ichetovkin, I., Grant, W., and Condeelis, J. (2002). Cofilin produces newly polymerized actin filaments that are preferred for dendritic nucleation by the Arp2/3 complex. Curr. Biol. **12,** 79-84.

Jiang, K., Sorefan, K., Deeks, M.J., Bevan, M.W., Hussey, P.J., and Hetherington, A.M. (2012). The ARP2/3 complex mediates guard cell actin reorganization and stomatal movement in *Arabidopsis*. Plant Cell **24,** 2031-2040.

Kadzik, R.S., Homa, K.E., and Kovar, D.R. (2020). F-actin cytoskeleton network self-organization through competition and cooperation. Annu. Rev. Cell Dev. Biol. **36,** 35-60.

Kovar, D.R. (2006). Molecular details of formin-mediated actin assembly. Curr. Opin. Cell Biol. **18,** 11-17.

Kovar, D.R., and Pollard, T.D. (2004). Progressing actin: Formin as a processive elongation machine. Nat. Cell Biol. **6,** 1158-1159.

Kovar, D.R., Kuhn, J.R., Tichy, A.L., and Pollard, T.D. (2003). The fission yeast cytokinesis formin Cdc12p is a barbed end actin filament capping protein gated by profilin. J. Cell Biol. **161,** 875-887.

Lan, Y., Liu, X., Fu, Y., and Huang, S. (2018). *Arabidopsis* class I formins control membrane-originated actin polymerization at pollen tube tips. PLOS Genet. **14,** e1007789.

Le, J., El-Assal, S.E.-D., Basu, D., Saad, M.E., and Szymanski, D.B. (2003). Requirements for *Arabidopsis* ATARP2 and ATARP3 during Epidermal Development. Curr. Biol. **13,** 1341-1347.

Li, J., and Staiger, C.J. (2018). Understanding Cytoskeletal Dynamics During the Plant Immune Response. Annu Rev Phytopathol **56,** 513-533.

Li, J., Henty-Ridilla, J.L., Huang, S., Wang, X., Blanchoin, L., and Staiger, C.J. (2012). Capping protein modulates the dynamic behavior of actin filaments in response to phosphatidic acid in *Arabidopsis*. Plant Cell **24,** 3742-3754.

Li, S., Blanchoin, L., Yang, Z., and Lord, E.M. (2003). The putative Arabidopsis Arp2/3 complex controls leaf cell morphogenesis. Plant Physiol. **132,** 2034-2044.

Li, X., Li, J.-H., Wang, W., Chen, N.-Z., Ma, T.-S., Xi, Y.-N., Zhang, X.-L., Lin, H.-F., Bai, Y., Huang, S.-J., and Chen, Y.-L. (2014). ARP2/3 complex-mediated actin dynamics is required for hydrogen peroxide-induced stomatal closure in Arabidopsis. Plant Cell Environ. **37,** 1548-1560.

Liu, H.-K., Li, Y.-J., Wang, S.-J., Yuan, T.-L., Huang, W.-J., Dong, X., Pei, J.-Q., Zhang, D., McCormick, S., and Tang, W.-H. (2020). Kinase partner protein plays a key role in controlling the speed and shape of pollen tube growth in tomato. Plant Physiol. **184,** 1853-1869.

Lomakin, A.J., Lee, K.-C., Han, S.J., Bui, D.A., Davidson, M., Mogilner, A., and Danuser, G. (2015). Competition for actin between two distinct F-actin networks defines a bistable switch for cell polarization. Nat. Cell Biol. **17,** 1435-1445.

Mathur, J., Mathur, N., Kernebeck, B., and Hulskamp, M. (2003a). Mutations in actin-related proteins 2 and 3 affect cell shape development in Arabidopsis. Plant Cell **15,** 1632-1645.

Mathur, J., Mathur, N., Kirik, V., Kernebeck, B., Srinivas, B.P., and Hulskamp, M. (2003b). *Arabidopsis* CROOKED encodes for the smallest subunit of the ARP2/3 complex and controls cell shape by region specific fine F-actin formation. Development **130,** 3137-3146.

Michelot, A., Grassart, A., Okreglak, V., Costanzo, M., Boone, C., and Drubin, D.G. (2013). Actin Filament Elongation in Arp2/3-Derived Networks Is Controlled by Three Distinct Mechanisms. Dev. Cell **24,** 182-195.

Michelot, A., Derivery, E., Paterski-Boujemaa, R., Guerin, C., Huang, S., Parcy, F., Staiger, C.J., and Blanchoin, L. (2006). A novel mechanism for the formation of actin-filament bundles by a nonprocessive formin. Curr. Biol. **16,** 1924-1930.

Michelot, A.e., Guérin, C., Huang, S., Ingouff, M., Richard, S.p., Rodiuc, N., Staiger, C.J., and Blanchoin, L. (2005). The formin homology 1 domain modulates the actin nucleation and bundling activity of Arabidopsis FORMIN1. Plant Cell **17,** 2296-2313.

Mullins, R.D., Heuser, J.A., and Pollard, T.D. (1998). The interaction of Arp2/3 complex with actin: Nucleation, high affinity pointed end capping, and formation of branching networks of filaments. Proc. Natl. Acad. Sci. USA **95,** 6181-6186.

Nishimura, Y., Shi, S., Li, Q., Bershadsky, A.D., and Viasnoff, V. (2021). Crosstalk between myosin II and formin functions in the regulation of force generation and actomyosin dynamics in stress fibers. Cells Dev. **168,** 203736.

Nolen, B.J., Tomasevic, N., Russell, A., Pierce, D.W., Jia, Z., McCormick, C.D., Hartman, J., Sakowicz, R., and Pollard, T.D. (2009). Characterization of two classes of small molecule inhibitors of Arp2/3 complex. Nature **460,** 1031-1034.

Orman, M., Landis, M., Oza, A., Nambiar, D., Gjeci, J., Song, K., Huang, V., Klestzick, A., Hachicho, C., Liu, S.Q., Kamm, J.M., Bartolini, F., Vadakkan, J.J., Rojas, C.M., and Vizcarra, C.L. (2022). Alterations to the broad-spectrum formin inhibitor SMIFH2 improve potency (Cold Spring Harbor Laboratory).

Paul, A.S., and Pollard, T.D. (2008). The role of the FH1 domain and profilin in formin-mediated actin-filament elongation and nucleation. Curr. Biol. **18,** 9-19.

Peng, X., Yan, T., and Sun, M. (2017). The WASP-Arp2/3 complex signal cascade is involved in actin-dependent sperm nuclei migration during double fertilization in tobacco and maize. Sci. Rep. **7,** 43161.

Peremyslov, V.V., Cole, R.A., Fowler, J.E., and Dolja, V.V. (2015). Myosin-Powered Membrane Compartment Drives Cytoplasmic Streaming, Cell Expansion and Plant Development. PLoS One **10,** e0139331.

Pollard, T.D. (2007). Regulation of actin filament assembly by Arp2/3 complex and formins. Annu. Rev. Biophys. Biomol. Struct. **36,** 451-477.

Pollard, T.D., Blanchoin, L., and Mullins, R.D. (2000). Molecular mechanisms controlling actin filament dynamics in nonmuscle cells. Annu. Rev. Biophys. Biomol. Struct. **29,** 545-576.

Qi, J., and Greb, T. (2017). Cell polarity in plants: the Yin and Yang of cellular functions. Curr. Opin. Plant Biol. **35,** 105-110.

Qin, L., Liu, L., Tu, J., Yang, G., Wang, S., Quilichini, T.D., Gao, P., Wang, H., Peng, G., Blancaflor, E.B., Datla, R., Xiang, D., Wilson, K.E., and Wei, Y. (2021). The ARP2/3 complex, acting cooperatively with Class I formins, modulates penetration resistance in Arabidopsis against powdery mildew invasion. Plant Cell **33,** 3151-3175.

Roh-Johnson, M., and Goldstein, B. (2009). In vivo roles for Arp2/3 in cortical actin organization during *C. elegans* gastrulation. J. Cell Sci. **122,** 3983-3993.

Romero, S., Le Clainche, C., Didry, D., Egile, C., Pantaloni, D., and Carlier, M.-F. (2004). Formin is a processive motor that requires profilin to accelerate actin assembly and associated ATP hydrolysis. Cell **119,** 419-429.

Rosenbloom, A.D., Kovar, E.W., Kovar, D.R., Loew, L.M., and Pollard, T.D. (2021). Mechanism of actin filament nucleation. Biophysical Journal **120,** 4399-4417.

Rosero, A., Žárský, V., and Cvrčková, F. (2013). AtFH1 formin mutation affects actin filament and microtubule dynamics in *Arabidopsis thaliana*. J. Exp. Bot. **64,** 585-597.

Rouiller, I., Xu, X.-P., Amann, K.J., Egile, C., Nickell, S., Nicastro, D., Li, R., Pollard, T.D., Volkmann, N., and Hanein, D. (2008). The structural basis of actin filament branching by the Arp2/3 complex. The Journal of Cell Biology **180,** 887-895.

Sahi, V.P., Cifrová, P., García-González, J., Kotannal Baby, I., Mouillé, G., Gineau, E., Müller, K., Baluška, F.e., Soukup, A., Petrášek, J., and Schwarzerová, K.i. (2018). *Arabidopsis thaliana* plants lacking the ARP2/3 complex show defects in cell wall assembly and auxin distribution. Ann. Bot. **122,** 777-789.

Sampathkumar, A., Gutierrez, R., McFarlane, H.E., Bringmann, M., Lindeboom, J., Emons, A.M., Samuels, L., Ketelaar, T., Ehrhardt, D.W., and Persson, S. (2013). Patterning and lifetime of plasma membrane-localized cellulose synthase is dependent on actin organization in Arabidopsis interphase cells. Plant Physiol **162,** 675-688.

Scheuring, D., Lofke, C., Kruger, F., Kittelmann, M., Eisa, A., Hughes, L., Smith, R.S., Hawes, C., Schumacher, K., and Kleine-Vehn, J. (2016). Actin-dependent vacuolar occupancy of the cell determines auxin-induced growth repression. Proc Natl Acad Sci U S A **113,** 452-457.

Sept, D., and McCammon, J.A. (2001). Thermodynamics and kinetics of actin filament nucleation. Biophys. J. **81,** 667-674.

Sheahan, M.B., Staiger, C.J., Rose, R.J., and McCurdy, D.W. (2004). A green fluorescent protein fusion to actin-binding domain 2 of Arabidopsis fimbrin highlights new features of a dynamic actin cytoskeleton in live plant cells. Plant Physiol. **136,** 3968-3978.

Staiger, C.J., Poulter, N.S., Henty, J.L., Franklin-Tong, V.E., and Blanchoin, L. (2010). Regulation of actin dynamics by actin-binding proteins in pollen. J. Exp. Bot. **61,** 1969-1986.

Staiger, C.J., Sheahan, M.B., Khurana, P., Wang, X., McCurdy, D.W., and Blanchoin, L. (2009). Actin filament dynamics are dominated by rapid growth and severing activity in the *Arabidopsis* cortical array. the Journal of Cell Biology **184,** 269-280.

Suarez, C., Carroll, R.T., Burke, T.A., Christensen, J.R., Bestul, A.J., Sees, J.A., James, M.L., Sirotkin, V., and Kovar, D.R. (2015). Profilin regulates F-actin network homeostasis by favoring formin over Arp2/3 complex. Dev. Cell **32,** 43-53.

Sun, S.-C., Wang, Q.-L., Gao, W.-W., Xu, Y.-N., Liu, H.-L., Cui, X.-S., and Kim, N.-H. (2013). Actin nucleator Arp2/3 complex is essential for mouse preimplantation embryo development. Reprod. Fertil. Dev. **25,** 617-623.

Szymanski, D.B., Marks, M.D., and Wick, S.M. (1999). Organized F-actin is essential for normal trichome morphogenesis in Arabidopsis. Plant Cell **11,** 2331-2347.

Ueda, H., Yokota, E., Kutsuna, N., Shimada, T., Tamura, K., Shimmen, T., Hasezawa, S., Dolja, V.V., and Hara-Nishimura, I. (2010). Myosin-dependent endoplasmic reticulum motility and F-actin organization in plant cells. Proc. Natl. Acad. Sci. USA **107,** 6894-6899.

van der Kammen, R., Song, J.-Y., de Rink, I., Janssen, H., Madonna, S., Scarponi, C., Albanesi, C., Brugman, W., and Innocenti, M. (2017). Knockout of the Arp2/3 complex in epidermis causes a psoriasis-like disease hallmarked by hyperactivation of transcription factor Nrf2. Development **144,** 4588-4603.

Vaškovičová, K., Žárský, V., Rösel, D., Nikolič, M., Buccione, R., Cvrčková, F., and Brábek, J. (2013). Invasive cells in animals and plants: searching for LECA machineries in later eukaryotic life. Biol. Direct **8,** 8.

Vavylonis, D., Kovar, D.R., O'Shaughnessy, B., and Pollard, T.D. (2006). Model of formin-associated actin filament elongation. Mol. Cell **21,** 455-466.

Vidali, L., van Gisbergen, P.A.C., Guerin, C., Franco, P., Li, M., Burkart, G.M., Augustine, R.C., Blanchoin, L., and Bezanilla, M. (2009). Rapid formin-mediated actin-filament elongation is essential for polarized plant cell growth. Proc. Natl. Acad. Sci. USA **106,** 13341-13346.

Wang, P., Richardson, C., Hawes, C., and Hussey, P.J. (2016). *Arabidopsis* NAP1 Regulates the Formation of Autophagosomes. Curr. Biol. **26,** 2060-2069.

Wang, P., Pleskot, R., Zang, J., Winkler, J., Wang, J., Yperman, K., Zhang, T., Wang, K., Gong, J., Guan, Y., Richardson, C., Duckney, P., Vandorpe, M., Mylle, E., Fiserova, J., Van Damme, D., and Hussey, P.J. (2019). Plant AtEH/Pan1 proteins drive autophagosome formation at ER-PM contact sites with actin and endocytic machinery. Nat. Commun. **10,** 5132.

Yanagisawa, M., Zhang, C., and Szymanski, D.B. (2013). ARP2/3-dependent growth in the plant kingdom: SCARs for life. Front. Plant Sci. **4,** 166.

Yanagisawa, M., Alonso, J.M., and Szymanski, D.B. (2018). Microtubule-dependent confinement of a cell signaling and actin polymerization control module regulates polarized cell growth. Curr. Biol. **28,** 2459-2466.e2454.

Yanagisawa, M., Desyatova, A.S., Belteton, S.A., Mallery, E.L., Turner, J.A., and Szymanski, D.B. (2015). Patterning mechanisms of cytoskeletal and cell wall systems during leaf trichome morphogenesis. Nat. Plants **1,** 15014.

Zhang, S., Liu, C., Wang, J., Ren, Z., Staiger, C.J., and Ren, H. (2016). A processive *Arabidopsis* formin modulates actin filament dynamics in association with profilin. Mol. Plant **9,** 900-910.

Zhang, W., Cai, C., and Staiger, C.J. (2019). Myosins XI are involved in exocytosis of cellulose synthase complexes. Plant Physiol. **179,** 1537-1555.

Zhang, W., Huang, L., Zhang, C., and Staiger, C.J. (2021). Arabidopsis myosin XIK interacts with the exocyst complex to facilitate vesicle tethering during exocytosis. Plant Cell **33,** 2454-2478.

Figure Legends

Figure 1 Disruption of the Arp2/3 complex leads to abnormal epidermal cell morphology and inhibits normal plant growth.

A, Representative images of epidermal cells from 5-d-old etiolated hypocotyls of homozygous *arp2/3* mutants, *arp2-1* and *arpc2*, and the respective wild-type lines (*ARP2* and *ARPC2*). Cells in *arp2-1* and *arpc2* seedlings had visible cell adhesion defects (yellow arrowheads) at end walls, shown by FM4-64 labeling of the plasma membrane, compared to wild-type sibling lines (top row). Bar = 10 μm. Representative images of trichomes from young leaves of 2-week-old plants (bottom row). Trichomes on *arp2-1* and *arpc2* leaves were severely distorted compared to the respective wild-type lines. Bar = 8 μm. B, Representative images of 5-d-old dark grown seedlings. Bar = 1.0 cm. C, Hypocotyls from *arp2-1* and *arpc2* were significantly shorter than the respective wild-type lines over a developmental timeseries. D and E, Quantitative analysis of average length (D) and width (E) of epidermal cells from the apical, middle, and basal regions of 5-d-old etiolated hypocotyls. F, Representative images of 5-d-old light grown seedlings of *ARP2*, *arp2-1*, *ARPC2* and *arpc2*. Bar = 1.0 cm. G, Roots from *arp2-1* and *arpc2* seedlings were significantly shorter than the respective wild-type lines over a developmental timeseries. Data shown are from one representative experiment of three biological repeats conducted with independent plant materials. Values in (C) and (G) represent mean ± SE. n ≥ 50 seedlings per genotype (Student's t test, ** $P < 0.005$, *** $P < 0.001$). Values in (D) and (E) represent mean ± SE. n ≥ 300 cells from at least 10 hypocotyls per genotype (Student's t test, ** $P < 0.005$, *** $P < 0.001$).

Figure 2 Genetic disruption of the Arp2/3 complex leads to reduced actin filament density and bundling.

A, Representative images of epidermal cells from the apical region of 5-d-old etiolated hypocotyls expressing GFP-fABD2 imaged by variable angle epifluorescence microscopy (VAEM) are shown in the left columns. Bar = 20 μm. Regions of interest (yellow box) from figures at left were magnified and shown in the right columns. Bar = 5 um. B and C, Quantitative analysis of the percentage of occupancy or density of actin filament arrays (B) and the extent of filament bundling or skewness (C). Both the density and the bundling of actin arrays in *arp2-1* and *arpc2* cells were significantly decreased compared to those in the respective wild-type cells

(*ARP2* and *ARPC2*). D, Quantitative analysis of the average angle of actin filaments relative to the longitudinal axis of hypocotyl epidermal cells. There was no significant difference in the average angle of actin arrays between wild-type and mutant cells. Values in (B) to (D) represent mean ± SE. n ≥ 300 ROIs from at least 15 hypocotyls per genotype (One-way ANOVA with Tukey's post-hoc test, letters [a–b] denote genotypes that show statistically significant differences with other genotypes, $P < 0.05$). E, Quantitative analysis of the population distribution and average parallelness of actin filaments. There was no significant difference in the average parallelness of actin arrays between wild-type and mutant cells; however, the population distributions of *arp2-1* and *arpc2* were more left skewed compared to the respective wild type. n ≥ 300 ROIs from at least 15 hypocotyls per genotype (letters [a–b] denote genotypes that show statistically significant differences with other genotypes by Chi-squared test, $P < 0.05$). All data shown are from one representative experiment of three biological repeats conducted with independent plant materials.

Figure 3 Actin filament nucleation frequency is decreased by chemical or genetic inhibition of the Arp2/3 complex.

A, Representative time lapse series showing three subclasses of actin filament origin identified in hypocotyl epidermal cells: Actin filaments initiated *de novo* in the cytoplasm (top), from the side of a pre-existing filament (middle), or from the end of a pre-existing filament (bottom row). Blue dots; pre-existing filament. Magenta dots; new growing filament. Green arrowheads; nucleation site. Bar = 5 μm. B and C, Quantitative analysis of actin filament nucleation frequency. The overall nucleation frequency for each genotype or treatment was defined as the total number of filament origins per filament per minute in a 400 μm^2 region of interest. Total nucleation frequency (B) in mock-treated wild-type cells (*ARP2*) was significantly higher than mock-treated *arp2-1*, CK-666-treated wild-type, or CK-666-treated *arp2-1* cells. When filament origin events were categorized into *de novo*, side, and end populations (C), only the side-branching nucleation events showed a significant reduction in *arp2-1* and CK-666-treated cells compared to mock-treated wild type. Data shown are from one representative experiment of three biological repeats conducted with independent plant materials. Values in (B) and (C) represent mean ± SE. n ≥ 300 total events from at least 10 hypocotyls per treatment or genotype (One-way ANOVA with Tukey's post-hoc test, letters [a–d] denote treatments that show statistically significant differences with other treatments or genotypes, $P < 0.05$).

Figure 4 Actin filament dynamic properties are altered when the Arp2/3 complex is inhibited.

A, A representative actin filament tracked during the elongation phase (top) and another filament is fragmented into pieces during the severing phase (bottom). Magenta dots; actin filament. Green arrowhead; nucleation site. White asterisk; elongating filament end. Yellow arrows; severing events. Bar = 10 μm. B, Quantitative analysis of the population distribution and average elongation rate of actin filaments in hypocotyl epidermal cells. The average elongation rate of filaments from mock-treated wild-type cells was significantly lower than that in mock-treated *arp2-1*, CK-666-treated wild-type, and CK-666- treated *arp2-1* cells; the elongation rate distribution of mock-treated wild type had a single peak at 1.25 – 1.5 μm/s whereas the Arp2/3-inhibited groups had three peaks at 0.75 – 1.25 μm/s, 2.0 – 2.25 μm/s, and > 3 μm/s. n ≥ 50 single filaments from at least 10 hypocotyls per genotype or treatment (letters [a–b] denote genotypes or treatments that show statistically significant differences with other groups by Chi-squared test, $P < 0.05$). C, Average maximum length of side-branching filaments in mock-treated wild-type cells was significantly longer than that in mock-treated *arp2-1*, CK-666-treated wild-type, or CK-666-treated *arp2-1* cells; however, filaments that originated *de novo* or from pre-existing ends did not show any significant difference. D, Average maximum lifetime of side-branching filaments in mock-treated wild-type cells was significantly shorter than that in mock-treated *arp2-1*, CK-666-treated wild-type, or CK-666-treated *arp2-1* cells; however, filaments that originated *de novo* or from pre-existing ends did not show any significant difference. E, The severing frequency of side-branching filaments in mock-treated *arp2-1*, CK-666-treated wild-type, or CK-666-treated *arp2-1* cells was significantly lower than filaments from other origins in both wild-type and *arp2-1* cells despite the treatment type. Values in (C) to (E) represent mean ± SE. n ≥ 50 single filaments from at least 10 hypocotyls per treatment (One-way ANOVA with Tukey's post-hoc test, letters [a–d] denote treatments that show statistically significant differences with other treatments, $P < 0.05$). All data shown are from one representative experiment of three biological repeats conducted with independent plant materials.

Figure 5 A small molecule inhibitor of the Arp2/3 complex, CK-666, reduces actin filament density and bundling.

A, Representative images of epidermal cells from the apical region of 5-d-old etiolated hypocotyls are shown in the left column. Bar = 20 μm. Regions of interest (yellow box) were magnified and displayed in the right column. Bar = 5 um. Hypocotyls were treated with mock solution (0.05% DMSO) or 10 μM CK-666 for 5 min prior to imaging with VAEM. Actin filament arrays in mock-treated *arp2-1*, CK-666-treated *ARP2*, and CK-666-treated *arp2-1* cells appeared to be less dense and less bundled compared to mock-treated wild-type cells. B and C, Quantitative analysis of the percentage of occupancy or density of actin filament arrays (B) and the extent of filament bundling or skewness (C). Both the density and bundling of actin arrays in mock-treated *arp2-1*, CK-666-treated wild type, and CK-666-treated *arp2-1* cells were significantly decreased compared to mock-treated wild-type cells. Values in (B) to (C) represent mean ± SE. n ≥ 300 ROIs from at least 15 hypocotyls per treatment or genotype (One-way ANOVA with Tukey's post-hoc test, letters [a–c] denote treatments or genotypes that show statistically significant differences with others, $P < 0.05$). D, Quantitative analysis of the population distribution and average parallelness of actin filaments in hypocotyl epidermal cells. The average filament parallelness of CK-666-treated wild-type cells (*ARP2*) was significantly higher than others. In addition, the population distribution of mock-treated *arp2-1*, CK-666-treated wild type, and CK-666-treated *arp2-1* was more left skewed compared to the mock-treated wild type. n ≥ 300 ROIs from at least 15 hypocotyls per genotype/treatment (letters [a–b] denote genotypes or treatments that show statistically significant differences with other groups by Chi-squared test, $P < 0.05$). All data shown are from one representative experiment of three biological repeats conducted with independent plant materials.

Figure 6 Actin filament density increases after treatment of *arp2-1* with the formin inhibitor SMIFH2.

A, Representative images of epidermal cells from the apical region of 5-d-old etiolated hypocotyls are shown in the left column. Bar = 20 μm. Regions of interest (yellow box) were magnified and displayed in the right column. Bar = 5 um. Hypocotyls were treated with mock solution (0.05% DMSO) or 25 μM SMIFH2 for 5 min prior to imaging with VAEM. Actin filament arrays in mock-treated *arp2-1*, CK-666-treated *ARP2*, and CK-666-treated *arp2-1* cells appeared to be less dense and less bundled compared to mock-treated wild-type cells. B to C, Quantitative analysis of density (B) and skewness (C). The density of actin arrays in mock-treated *arp2-1* and SMIFH2-treated wild type was significantly decreased compared to mock-

treated wild type; however, SMIFH2-treated *arp2-1* cells had significantly increased actin density compared to other genotypes and treatments. C, Actin arrays in *arp2-1* cells were significantly less bundled compared to wild-type cells (both mock- and SMIFH2-treated). Values in (B) to (C) represent mean ± SE. n ≥ 300 ROIs from at least 15 hypocotyls per treatment (One-way ANOVA with Tukey's post-hoc test, letters [a–d] denote treatments or genotypes that show statistically significant differences with others, $P < 0.05$). D, Quantitative analysis of the population distribution and average parallelness of actin filaments. The average parallelness of actin filaments in SMIFH2-treated wild-type cells was slightly higher than other genotypes and treatments; however, the distribution of SMIFH2-treated *arp2-1* was more right skewed compared to other genotypes and treatments. n ≥ 300 ROIs from at least 10 hypocotyls per genotype or treatment (letters [a–d] denote genotypes or treatments that show statistically significant differences with other groups by Chi-squared test, $P < 0.05$). All data shown are from one representative experiment of three biological repeats conducted with independent plant materials.

Figure 7 Overall and *de novo* filament formation increase when Arp2/3 and formin activity are simultaneously inhibited.

A, Quantitative analysis of actin filament nucleation frequency, both overall and by subclass of origin. The total nucleation frequency in mock-treated *arp2-1* and SMIFH2-treated wild-type cells was significantly reduced compared to mock-treated wild-type (*ARP2*) cells. However, the total nucleation frequency of SMIFH2-treated *arp2-1* cells was significantly higher than all other genotypes and treatments and this correlated with increased *de novo* nucleation events. Values represent mean ± SE. n ≥ 300 total events from at least 10 hypocotyls per treatment or genotype (One-way ANOVA with Tukey's post-hoc test, letters [a–f] denote treatments or genotypes that show statistically significant differences with others, $P < 0.05$). B, Average maximum length of filaments that originated *de novo* or from side-branching events in SMIFH2-treated *arp2-1* was significantly shorter than that in other cells, but filaments that originated from pre-existing ends did not show a difference between any genotype or treatment. C, Average maximum lifetime of side-branching filaments in both mock-treated *arp2-1* and SMIFH2-treated wild-type was significantly longer than the ones from mock-treated wild-type and SMIFH2-treated *arp2-1* cells. Filaments that were nucleated *de novo* in SMIFH2-treated *arp2-1* cells were significantly shorter than *de novo* filaments from other genotypes or treatments. D, Side-

branching filaments in mock-treated wild-type cells had a significantly higher severing frequency than the ones from other cells and end-growing filaments in both SMIFH2-treated wild-type and SMIFH2-treated *arp2-1* cells had significantly higher severing frequency than the ones from mock-treated cells. Values in (B) to (D) represent mean ± SE. n ≥ 50 single filaments from at least 10 hypocotyls per treatment (One-way ANOVA with Tukey's post-hoc test, letters [a–d] denote treatments that show statistically significant differences with other treatments, $P < 0.05$). E, Analysis of the population distribution of actin filament elongation rates. The average elongation rate for filaments from mock-treated *arp2-1*, SMIFH2-treated wild-type, and SMIFH2-treated *arp2-1* cells was significantly higher than mock-treated wild type. The elongation rate distribution of mock-treated wild type had a single peak at 1.25 – 1.5 μm/s, the mock-treated *arp2-1* had three peaks at 0.75 – 1.0 μm/s, 2.0 – 2.25 μm/s and > 3 μm/s, the SMIFH2-treated wild-type had a peak at 1.0 – 1.25 μm/s, but SMIFH2-treated *arp2-1* had peaks at 1.0 – 1.25 μm/s and 1.75 – 2.0 μm/s. n ≥ 50 single filaments from at least 10 hypocotyls per genotype/treatment (letters [a–d] denote genotypes/treatments that show statistically significant differences with other groups by Chi-squared test, $P < 0.05$). All data shown are from one representative experiment of three biological repeats conducted with independent plant materials.

Figure 8 Filament abundance, total nucleation events and *de novo* filament formation increase when the Arp2/3 complex and formin activity are simultaneously reduced with inhibitors.

A, Representative images of Col-0 hypocotyl epidermal cells expressing GFP-fABD2 after treatment with mock solution (0.1% DMSO), 10 μM CK-666, 25 μM SMIFH2, or both CK-666 and SMIFH2 for 5 min prior to imaging with VAEM. Actin filament arrays in CK-666-treated cells and SMIFH2-treated cells appeared to be less dense and less bundled compared to mock-treated cells. However, dual treatment markedly increased actin filament abundance. Bar = 10 μm. B, Quantitative analysis of actin filament nucleation frequency, both overall and by subclass of origin. The total nucleation frequency in mock-treated cells was higher than CK-666-treated and SMIFH2-treated cells. However, the total nucleation frequency of dual-treated cells was significantly higher than other treatments and this correlated with increased *de novo* and side-branching nucleation events. Values in (B) represent mean ± SE. n ≥ 300 total events from at least 10 hypocotyls per treatment (One-way ANOVA with Tukey's post-hoc test, letters [a–g] denote treatments that show statistically significant differences with other treatments, $P < 0.05$).

C and D, Quantitative analysis of density (C) and skewness (D) of actin filaments. (C) The density of actin arrays in CK-666-treated and SMIFH2-treated cells was decreased compared to mock-treated cells; however, dual-treated cells had significantly increased actin density compared to other treatments. (D) Actin arrays in CK-666- or dual-treated cells were significantly less bundled than in mock-treated cells. Values in (C) and (D) represent mean ± SE. n ≥ 300 ROIs from at least 15 hypocotyls per treatment (One-way ANOVA with Tukey's post-hoc test, letters [a–d] denote treatments that show statistically significant differences with other treatments, $P < 0.05$). All data shown are from one representative experiment of three biological repeats conducted with independent plant materials.

Figures & Figure Legends

Table 1. Single actin filament dynamics in wild type (*ARP2*) and *arp2-1* mutant with or without CK-666.

Stochastic Dynamic Parameters	Genotype & Treatment			
	ARP2 w/ mock	*arp2-1* w/ mock	*ARP2* w/ CK-666	*arp2-1* w/ CK-666
Elongation Rate; µm/s	1.75 ± 0.09 [a]	1.89 ± 0.10 [b]	1.91 ± 0.10 [b]	1.91 ± 0.10 [b]
Max. Filament Length; µm	16.5 ± 0.3 [a]	17.1 ± 0.2 [b]	17.0 ± 0.2 [b]	17.3 ± 0.4 [b]
Max. Filament Lifetime; s	23.1 ± 0.4 [a]	23.1 ± 0.4 [a]	23.0 ± 0.5 [a]	22.9 ± 0.4 [a]
Severing Frequency; breaks/mm/s	8.14 ± 0.22 [a]	8.07 ± 0.18 [a]	7.94 ± 0.27 [b]	8.11 ± 0.25 [a]

Measurements were taken from the elongation apical region of 5-d-old dark-grown hypocotyls. Data shown are from one representative experiment of three biological repeats conducted with independent plant materials.
Values represent mean ± SE. n ≥ 50 filaments from at least 10 hypocotyls per treatment. One-way ANOVA with Tukey's post-hoc test, letters [a–b] denote genotypes or treatments that show statistically significant differences with other genotypes or treatments, $P < 0.05$

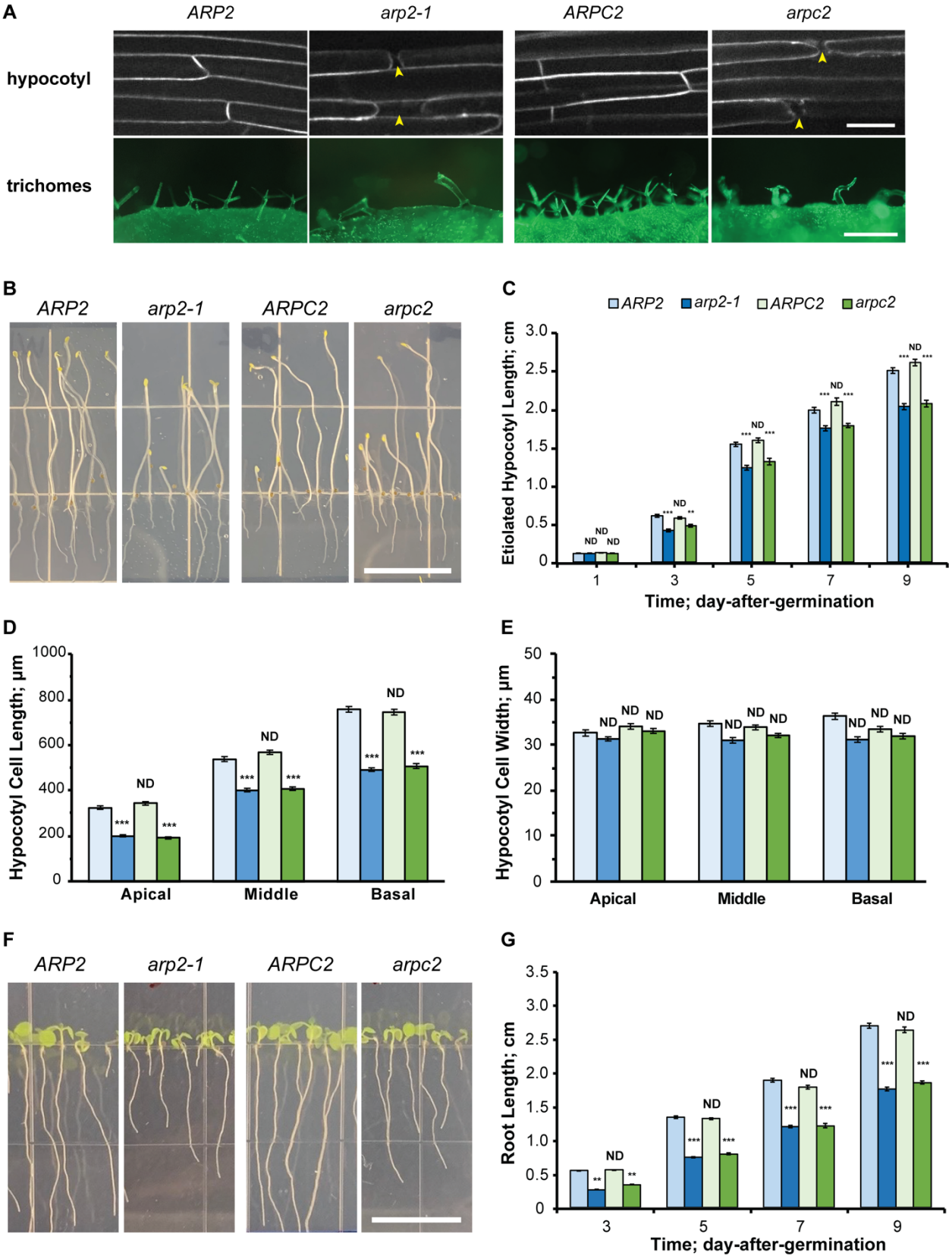
A
ARP2
arp2-1
ARPC2
arpc2
hypocotyl
trichomes
B
ARP2
arp2-1
ARPC2
arpc2
C
ARP2
arp2-1
ARPC2
arpc2
Etiolated Hypocotyl Length; cm
Time; day-after-germination
D
Hypocotyl Cell Length; µm
Apical
Middle
Basal
E
Hypocotyl Cell Width; µm
Apical
Middle
Basal
F
ARP2
arp2-1
ARPC2
arpc2
G
Root Length; cm
Time; day-after-germination

Figure 1 Disruption of the Arp2/3 complex leads to abnormal epidermal cell morphology and inhibits normal plant growth.

A, Representative images of epidermal cells from 5-d-old etiolated hypocotyls of homozygous *arp2/3* mutants, *arp2-1* and *arpc2*, and the respective wild-type lines (*ARP2* and *ARPC2*). Cells in *arp2-1* and *arpc2* seedlings had visible cell adhesion defects (yellow arrowheads) at end walls, shown by FM4-64 labeling of the plasma membrane, compared to wild-type sibling lines (top row). Bar = 10 µm. Representative images of trichomes from young leaves of 2-week-old plants (bottom row). Trichomes on *arp2-1* and *arpc2* leaves were severely distorted compared to the respective wild-type lines. Bar = 8 µm. B, Representative images of 5-d-old dark grown seedlings. Bar = 1.0 cm. C, Hypocotyls from *arp2-1* and *arpc2* were significantly shorter than the respective wild-type lines over a developmental timeseries. D and E, Quantitative analysis of average length (D) and width (E) of epidermal cells from the apical, middle, and basal regions of 5-d-old etiolated hypocotyls. F, Representative images of 5-d-old light grown seedlings of *ARP2*, *arp2-1*, *ARPC2* and *arpc2*. Bar = 1.0 cm. G, Roots from *arp2-1* and *arpc2* seedlings were significantly shorter than the respective wild-type lines over a developmental timeseries. Data shown are from one representative experiment of three biological repeats conducted with independent plant materials. Values in (C) and (G) represent mean ± SE. $n \geq 50$ seedlings per genotype (Student's t test, ** $P < 0.005$, *** $P < 0.001$). Values in (D) and (E) represent mean ± SE. $n \geq 300$ cells from at least 10 hypocotyls per genotype (Student's t test, ** $P < 0.005$, *** $P < 0.001$).

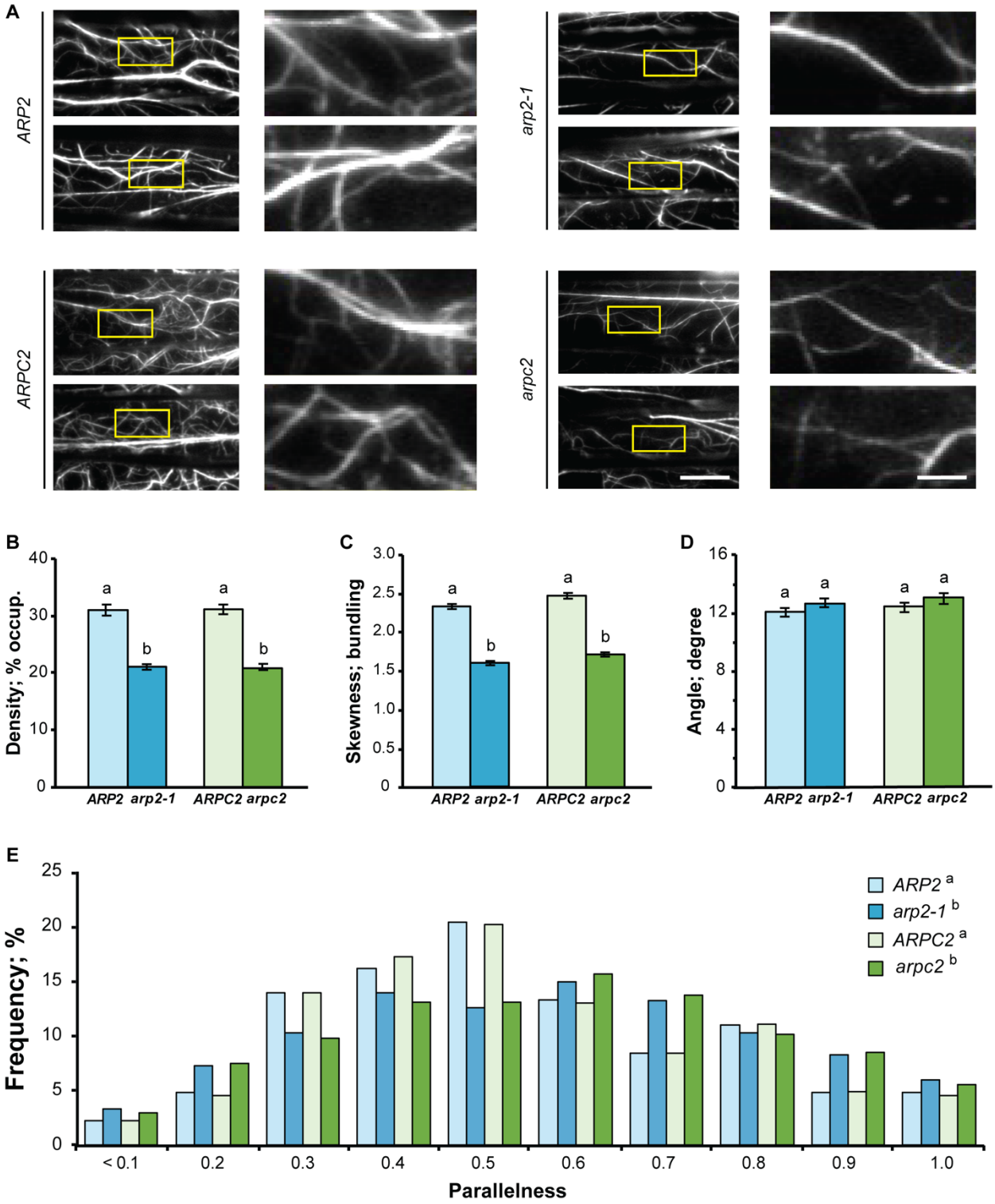
A
ARP2
arp2-1
ARPC2
arpc2
B
Density; % occup.
40
30
20
10
0
a
b
a
b
ARP2 arp2-1 ARPC2 arpc2
C
Skewness; bundling
3.0
2.5
2.0
1.5
1.0
0.5
0
a
b
a
b
ARP2 arp2-1 ARPC2 arpc2
D
Angle; degree
16
12
8
4
0
a
a
a
a
ARP2 arp2-1 ARPC2 arpc2
E
Frequency; %
25
20
15
10
5
0
ARP2 a
arp2-1 b
ARPC2 a
arpc2 b
< 0.1
0.2
0.3
0.4
0.5
0.6
0.7
0.8
0.9
1.0
Parallelness

Figure 2 Genetic disruption of the Arp2/3 complex leads to reduced actin filament density and bundling.

A, Representative images of epidermal cells from the apical region of 5-d-old etiolated hypocotyls expressing GFP-fABD2 imaged by variable angle epifluorescence microscopy (VAEM) are shown in the left columns. Bar = 20 µm. Regions of interest (yellow box) from figures at left were magnified and shown in the right columns. Bar = 5 um. B and C, Quantitative analysis of the percentage of occupancy or density of actin filament arrays (B) and the extent of filament bundling or skewness (C). Both the density and the bundling of actin arrays in *arp2-1* and *arpc2* cells were significantly decreased compared to those in the respective wild-type cells (*ARP2* and *ARPC2*). D, Quantitative analysis of the average angle of actin filaments relative to the longitudinal axis of hypocotyl epidermal cells. There was no significant difference in the average angle of actin arrays between wild-type and mutant cells. Values in (B) to (D) represent mean ± SE. $n \geq 300$ ROIs from at least 15 hypocotyls per genotype (One-way ANOVA with Tukey's post-hoc test, letters [a–b] denote genotypes that show statistically significant differences with other genotypes, $P < 0.05$). E, Quantitative analysis of the population distribution and average parallelness of actin filaments. There was no significant difference in the average parallelness of actin arrays between wild-type and mutant cells; however, the population distributions of *arp2-1* and *arpc2* were more left skewed compared to the respective wild type. $n \geq 300$ ROIs from at least 15 hypocotyls per genotype (letters [a–b] denote genotypes that show statistically significant differences with other genotypes by Chi-squared test, $P < 0.05$). All data shown are from one representative experiment of three biological repeats conducted with independent plant materials.

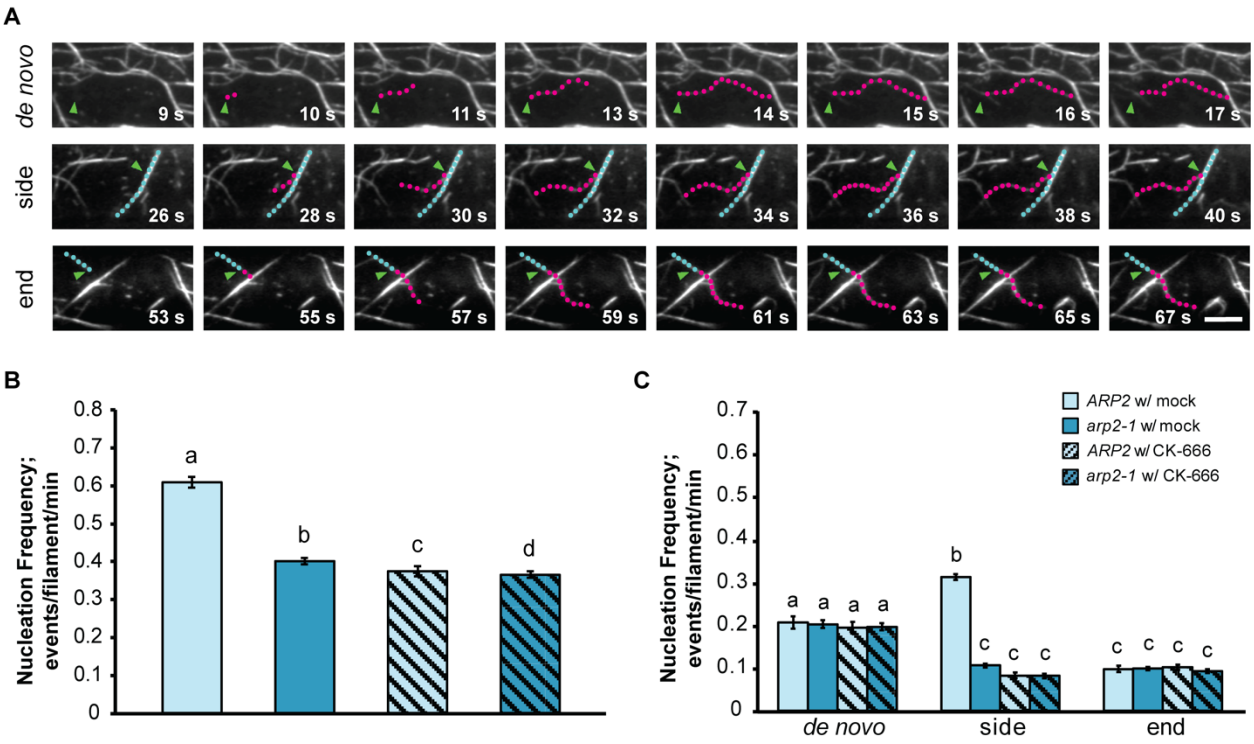

Figure 3 Actin filament nucleation frequency is decreased by chemical or genetic inhibition of the Arp2/3 complex.

A, Representative time lapse series showing three subclasses of actin filament origin identified in hypocotyl epidermal cells: Actin filaments initiated *de novo* in the cytoplasm (top), from the side of a pre-existing filament (middle), or from the end of a pre-existing filament (bottom row). Blue dots; pre-existing filament. Magenta dots; new growing filament. Green arrowheads; nucleation site. Bar = 5 µm. B and C, Quantitative analysis of actin filament nucleation frequency. The overall nucleation frequency for each genotype or treatment was defined as the total number of filament origins per filament per minute in a 400 μm^2 region of interest. Total nucleation frequency (B) in mock-treated wild-type cells (*ARP2*) was significantly higher than mock-treated *arp2-1*, CK-666-treated wild-type, or CK-666-treated *arp2-1* cells. When filament origin events were categorized into *de novo*, side, and end populations (C), only the side-branching nucleation events showed a significant reduction in *arp2-1* and CK-666-treated cells compared to mock-treated wild type. Data shown are from one representative experiment of three biological repeats conducted with independent plant materials. Values in (B) and (C) represent mean ± SE. n ≥ 300 total events from at least 10 hypocotyls per treatment or genotype (One-way ANOVA with Tukey's post-hoc test, letters [a–d] denote treatments that show statistically significant differences with other treatments or genotypes, $P < 0.05$).

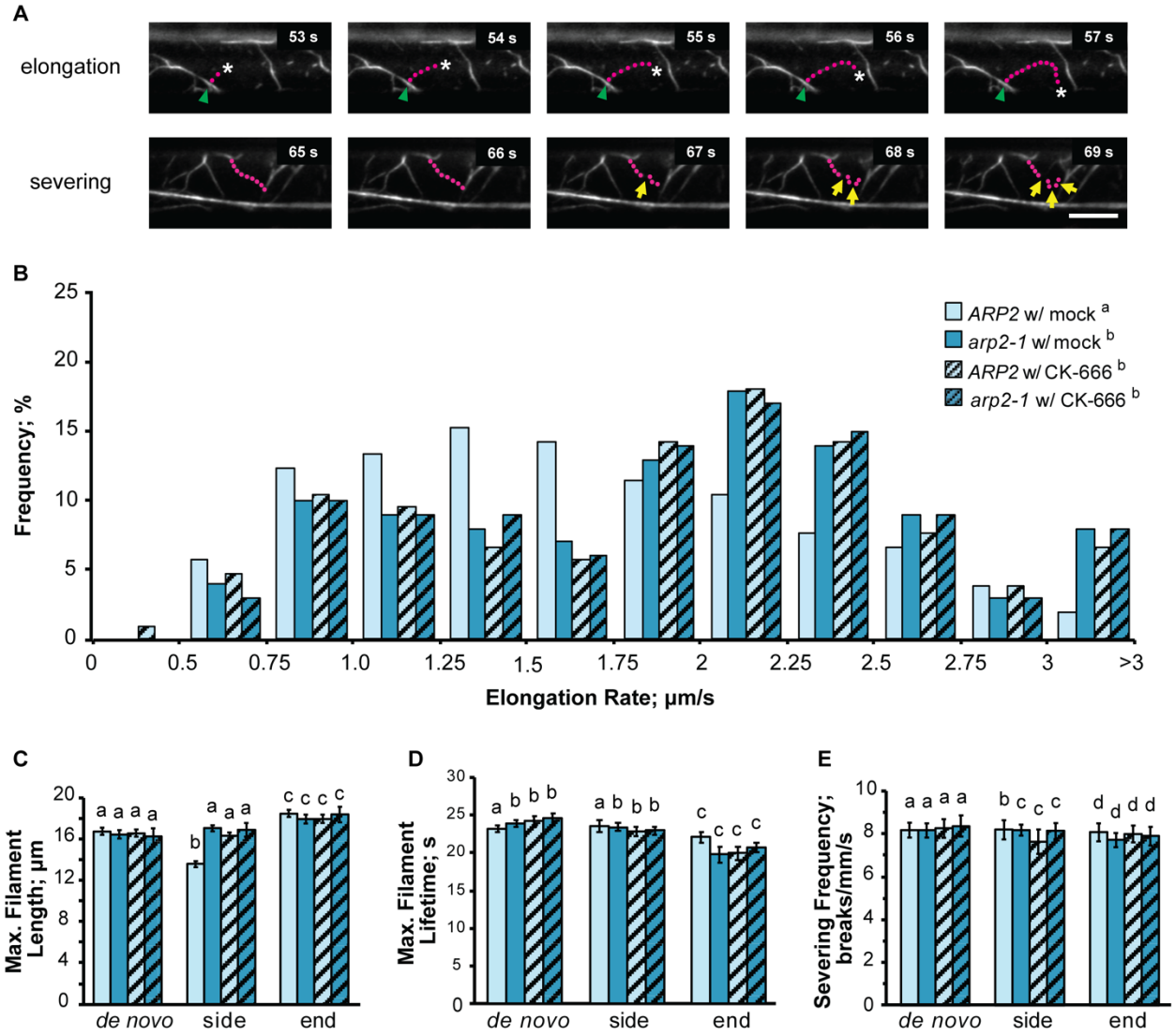

Figure 4 Actin filament dynamic properties are altered when the Arp2/3 complex is inhibited.

A, A representative actin filament tracked during the elongation phase (top) and another filament is fragmented into pieces during the severing phase (bottom). Magenta dots; actin filament. Green arrowhead; nucleation site. White asterisk; elongating filament end. Yellow arrows; severing events. Bar = 10 µm. B, Quantitative analysis of the population distribution and average elongation rate of actin filaments in hypocotyl epidermal cells. The average elongation rate of filaments from mock-treated wild-type cells was significantly lower than that in mock-treated *arp2-1*, CK-666-treated wild-type, and CK-666- treated *arp2-1* cells; the elongation rate distribution of mock-treated wild type had a single peak at 1.25 – 1.5 µm/s whereas the Arp2/3-inhibited groups had three peaks at 0.75 – 1.25 µm/s, 2.0 – 2.25 µm/s, and > 3 µm/s. n ≥ 50 single filaments from at least 10 hypocotyls per genotype or treatment (letters [a–b] denote genotypes or treatments that show statistically significant differences with other groups by Chi-squared test, $P < 0.05$). C, Average maximum length of side-branching filaments in mock-treated wild-type cells was significantly longer than that in mock-treated *arp2-1*, CK-666-treated wild-type, or CK-666-treated *arp2-1* cells; however, filaments that originated *de novo* or from pre-existing ends did not show any significant difference. D, Average maximum lifetime of side-branching filaments in mock-treated wild-type cells was significantly shorter than that in mock-treated *arp2-1*, CK-666-treated wild-

type, or CK-666-treated *arp2-1* cells; however, filaments that originated *de novo* or from pre-existing ends did not show any significant difference. E, The severing frequency of side-branching filaments in mock-treated *arp2-1*, CK-666-treated wild-type, or CK-666-treated *arp2-1* cells was significantly lower than filaments from other origins in both wild-type and *arp2-1* cells despite the treatment type. Values in (C) to (E) represent mean ± SE. $n \geq 50$ single filaments from at least 10 hypocotyls per treatment (One-way ANOVA with Tukey's post-hoc test, letters [a–d] denote treatments that show statistically significant differences with other treatments, $P < 0.05$). All data shown are from one representative experiment of three biological repeats conducted with independent plant materials.

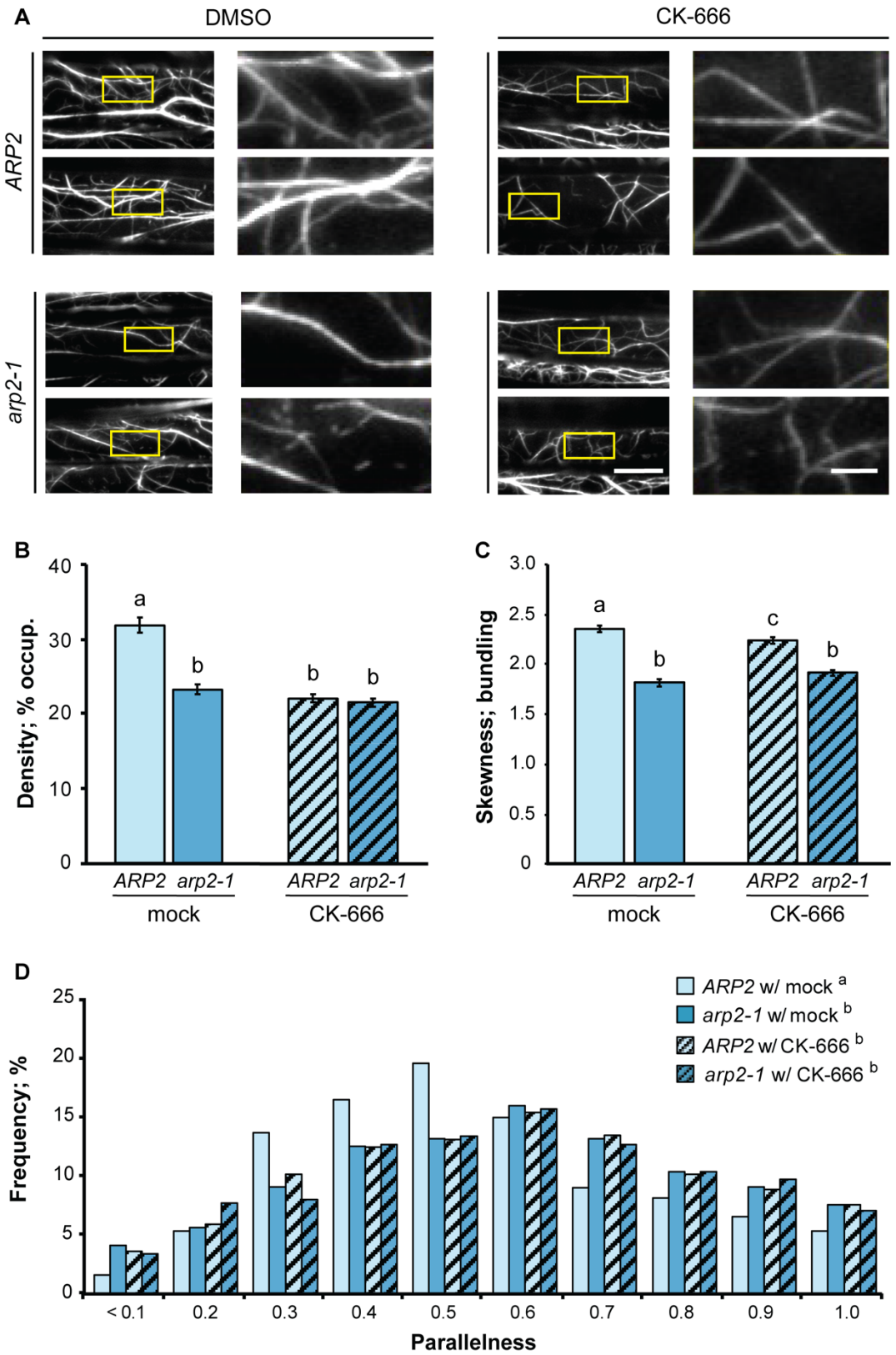
A
DMSO
CK-666
ARP2
arp2-1
B
Density; % occup.
40
30
20
10
0
a
b
b
b
ARP2
arp2-1
ARP2
arp2-1
mock
CK-666
C
Skewness; bundling
3.0
2.5
2.0
1.5
1.0
0.5
0
a
b
c
b
ARP2
arp2-1
ARP2
arp2-1
mock
CK-666
D
Frequency; %
25
20
15
10
5
0
ARP2 w/ mock a
arp2-1 w/ mock b
ARP2 w/ CK-666 b
arp2-1 w/ CK-666 b
< 0.1
0.2
0.3
0.4
0.5
0.6
0.7
0.8
0.9
1.0
Parallelness

Figure 5 A small molecule inhibitor of the Arp2/3 complex, CK-666, reduces actin filament density and bundling.

A, Representative images of epidermal cells from the apical region of 5-d-old etiolated hypocotyls are shown in the left column. Bar = 20 μm. Regions of interest (yellow box) were magnified and displayed in the right column. Bar = 5 um. Hypocotyls were treated with mock solution (0.05% DMSO) or 10 μM CK-666 for 5 min prior to imaging with VAEM. Actin filament arrays in mock-treated *arp2-1*, CK-666-treated *ARP2*, and CK-666-treated *arp2-1* cells appeared to be less dense and less bundled compared to mock-treated wild-type cells. B and C, Quantitative analysis of the percentage of occupancy or density of actin filament arrays (B) and the extent of filament bundling or skewness (C). Both the density and bundling of actin arrays in mock-treated *arp2-1*, CK-666-treated wild type, and CK-666-treated *arp2-1* cells were significantly decreased compared to mock-treated wild-type cells. Values in (B) to (C) represent mean ± SE. $n \geq 300$ ROIs from at least 15 hypocotyls per treatment or genotype (One-way ANOVA with Tukey's post-hoc test, letters [a–c] denote treatments or genotypes that show statistically significant differences with others, $P < 0.05$). D, Quantitative analysis of the population distribution and average parallelness of actin filaments in hypocotyl epidermal cells. The average filament parallelness of CK-666-treated wild-type cells (*ARP2*) was significantly higher than others. In addition, the population distribution of mock-treated *arp2-1*, CK-666-treated wild type, and CK-666-treated *arp2-1* was more left skewed compared to the mock-treated wild type. $n \geq 300$ ROIs from at least 15 hypocotyls per genotype/treatment (letters [a–b] denote genotypes or treatments that show statistically significant differences with other groups by Chi-squared test, $P < 0.05$). All data shown are from one representative experiment of three biological repeats conducted with independent plant materials.

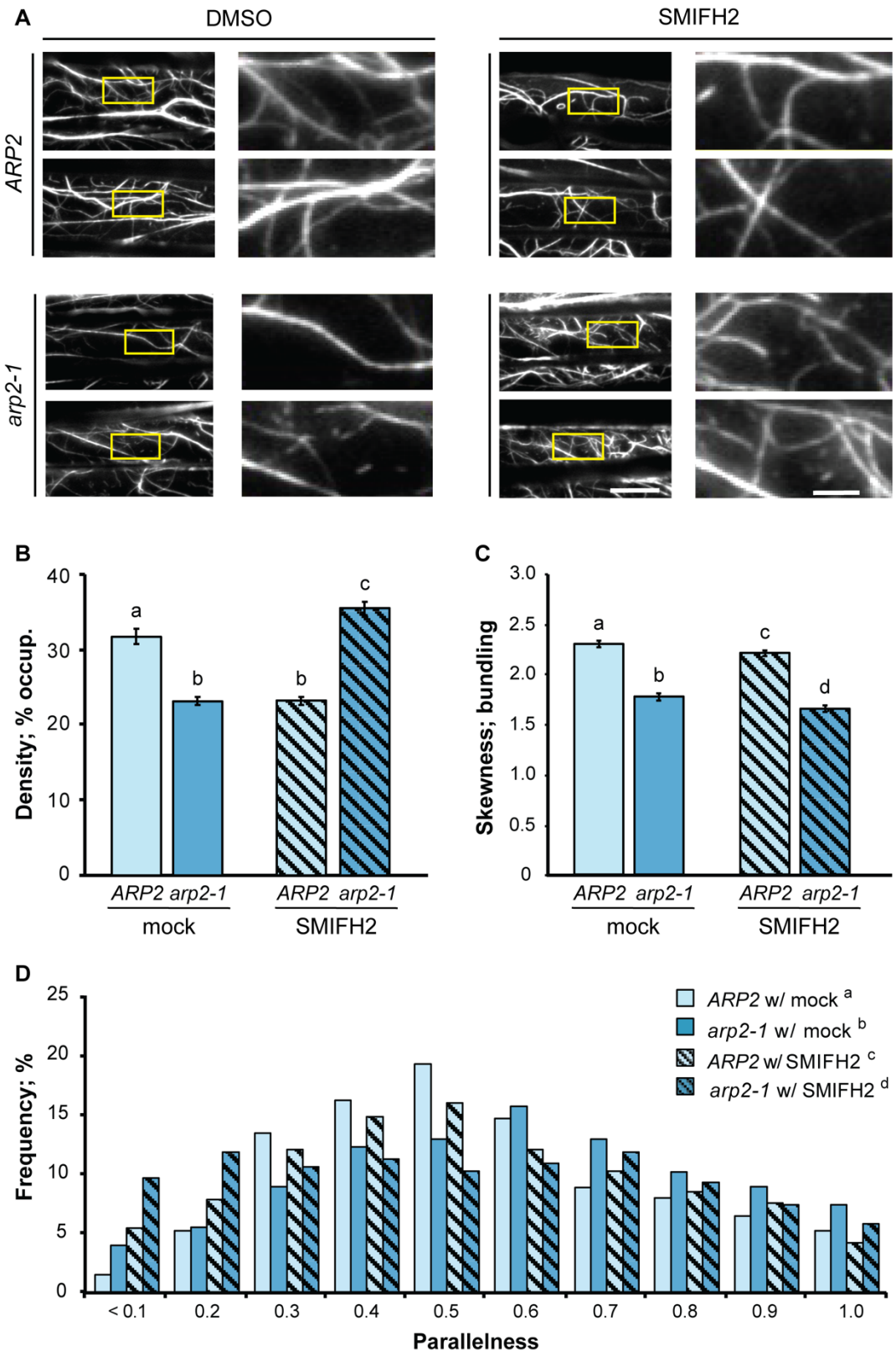
A
DMSO
SMIFH2
ARP2
arp2-1
B
Density; % occup.
40
30
20
10
0
a
b
b
c
ARP2 arp2-1
mock
ARP2 arp2-1
SMIFH2
C
Skewness; bundling
3.0
2.5
2.0
1.5
1.0
0.5
0
a
b
c
d
ARP2 arp2-1
mock
ARP2 arp2-1
SMIFH2
D
Frequency; %
25
20
15
10
5
0
ARP2 w/ mock a
arp2-1 w/ mock b
ARP2 w/ SMIFH2 c
arp2-1 w/ SMIFH2 d
< 0.1
0.2
0.3
0.4
0.5
0.6
0.7
0.8
0.9
1.0
Parallelness

Figure 6 Actin filament density increases after treatment of *arp2-1* with the formin inhibitor SMIFH2.

A, Representative images of epidermal cells from the apical region of 5-d-old etiolated hypocotyls are shown in the left column. Bar = 20 µm. Regions of interest (yellow box) were magnified and displayed in the right column. Bar = 5 um. Hypocotyls were treated with mock solution (0.05% DMSO) or 25 µM SMIFH2 for 5 min prior to imaging with VAEM. Actin filament arrays in mock-treated *arp2-1*, CK-666-treated *ARP2*, and CK-666-treated *arp2-1* cells appeared to be less dense and less bundled compared to mock-treated wild-type cells. B to C, Quantitative analysis of density (B) and skewness (C). The density of actin arrays in mock-treated *arp2-1* and SMIFH2-treated wild type was significantly decreased compared to mock-treated wild type; however, SMIFH2-treated *arp2-1* cells had significantly increased actin density compared to other genotypes and treatments. C, Actin arrays in *arp2-1* cells were significantly less bundled compared to wild-type cells (both mock- and SMIFH2-treated). Values in (B) to (C) represent mean ± SE. n ≥ 300 ROIs from at least 15 hypocotyls per treatment (One-way ANOVA with Tukey's post-hoc test, letters [a–d] denote treatments or genotypes that show statistically significant differences with others, $P < 0.05$). D, Quantitative analysis of the population distribution and average parallelness of actin filaments. The average parallelness of actin filaments in SMIFH2-treated wild-type cells was slightly higher than other genotypes and treatments; however, the distribution of SMIFH2-treated *arp2-1* was more right skewed compared to other genotypes and treatments. n ≥ 300 ROIs from at least 10 hypocotyls per genotype or treatment (letters [a–d] denote genotypes or treatments that show statistically significant differences with other groups by Chi-squared test, $P < 0.05$). All data shown are from one representative experiment of three biological repeats conducted with independent plant materials.

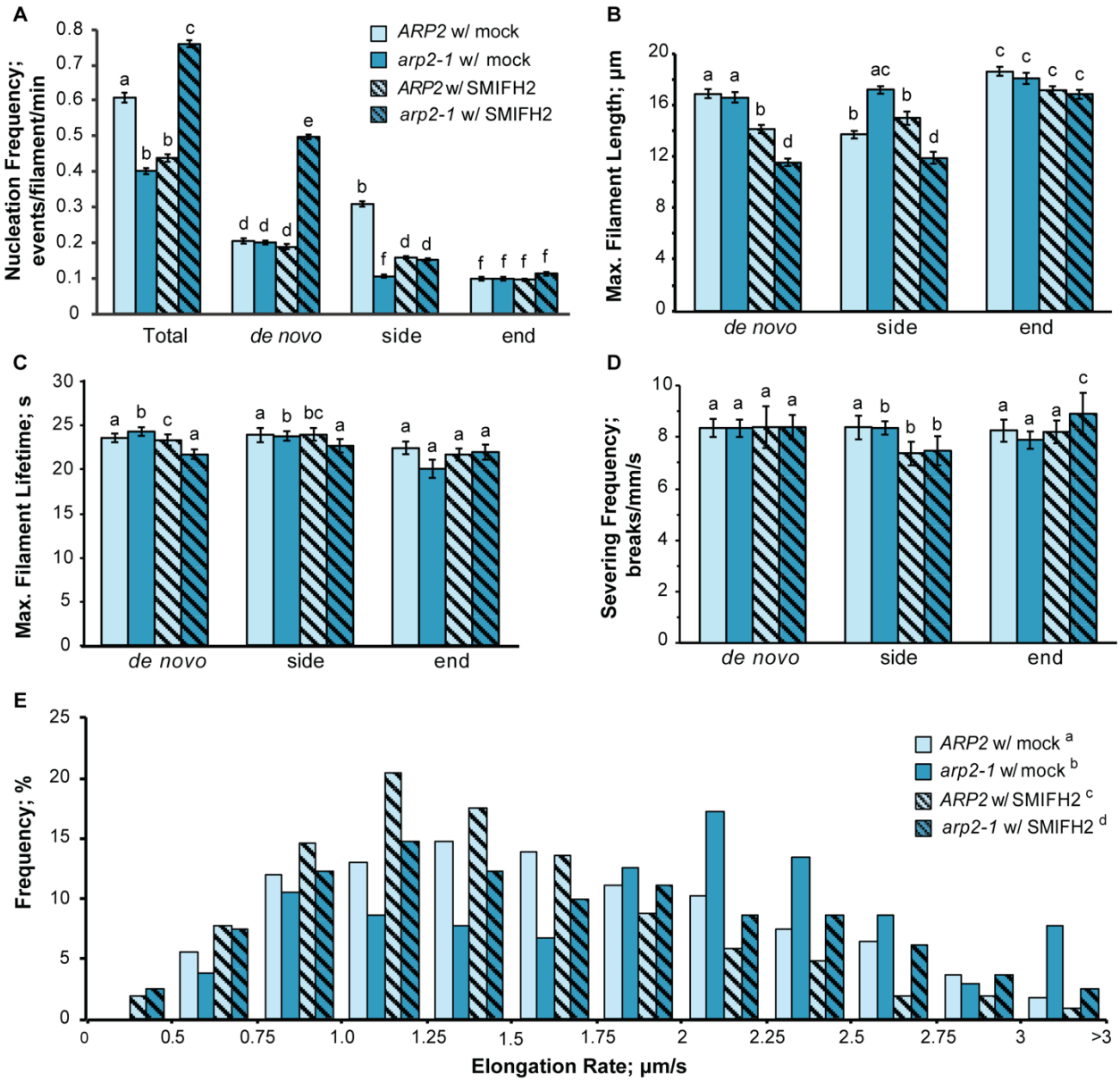

Figure 7 Overall and *de novo* filament formation increase when Arp2/3 and formin activity are simultaneously inhibited.

A, Quantitative analysis of actin filament nucleation frequency, both overall and by subclass of origin. The total nucleation frequency in mock-treated *arp2-1* and SMIFH2-treated wild-type cells was significantly reduced compared to mock-treated wild-type (*ARP2*) cells. However, the total nucleation frequency of SMIFH2-treated *arp2-1* cells was significantly higher than all other genotypes and treatments and this correlated with increased *de novo* nucleation events. Values represent mean ± SE. n ≥ 300 total events from at least 10 hypocotyls per treatment or genotype (One-way ANOVA with Tukey's post-hoc test, letters [a–f] denote treatments or genotypes that show statistically significant differences with others, $P < 0.05$). B, Average maximum length of filaments that originated *de novo* or from side-branching events in SMIFH2-treated *arp2-1* was significantly shorter than that in other cells, but filaments that originated from pre-existing ends did not show a difference between any genotype or treatment. C, Average maximum lifetime of side-branching filaments in both mock-treated *arp2-1* and

SMIFH2-treated wild-type was significantly longer than the ones from mock-treated wild-type and SMIFH2-treated *arp2-1* cells. Filaments that were nucleated *de novo* in SMIFH2-treated *arp2-1* cells were significantly shorter than *de novo* filaments from other genotypes or treatments. D, Side-branching filaments in mock-treated wild-type cells had a significantly higher severing frequency than the ones from other cells and end-growing filaments in both SMIFH2-treated wild-type and SMIFH2-treated *arp2-1* cells had significantly higher severing frequency than the ones from mock-treated cells. Values in (B) to (D) represent mean ± SE. $n \geq 50$ single filaments from at least 10 hypocotyls per treatment (One-way ANOVA with Tukey's post-hoc test, letters [a–d] denote treatments that show statistically significant differences with other treatments, $P < 0.05$). E, Analysis of the population distribution of actin filament elongation rates. The average elongation rate for filaments from mock-treated *arp2-1*, SMIFH2-treated wild-type, and SMIFH2-treated *arp2-1* cells was significantly higher than mock-treated wild type. The elongation rate distribution of mock-treated wild type had a single peak at 1.25 – 1.5 µm/s, the mock-treated *arp2-1* had three peaks at 0.75 – 1.0 µm/s, 2.0 – 2.25 µm/s and > 3 µm/s, the SMIFH2-treated wild-type had a peak at 1.0 – 1.25 µm/s, but SMIFH2-treated *arp2-1* had peaks at 1.0 – 1.25 µm/s and 1.75 – 2.0 µm/s. $n \geq 50$ single filaments from at least 10 hypocotyls per genotype/treatment (letters [a–d] denote genotypes/treatments that show statistically significant differences with other groups by Chi-squared test, $P < 0.05$). All data shown are from one representative experiment of three biological repeats conducted with independent plant materials.

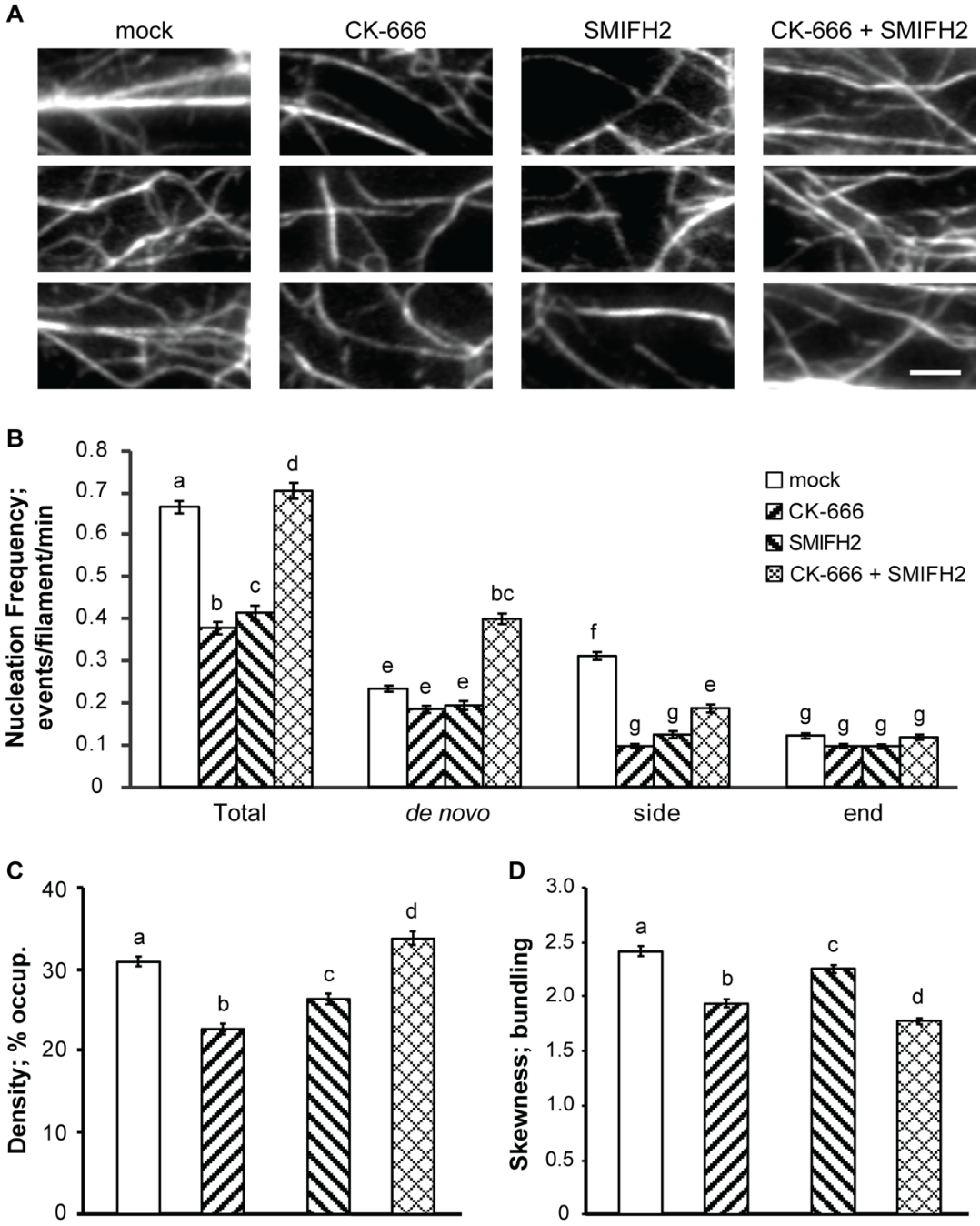

Figure 8 Filament abundance, total nucleation events and *de novo* filament formation increase when the Arp2/3 complex and formin activity are simultaneously reduced with inhibitors.

A, Representative images of Col-0 hypocotyl epidermal cells expressing GFP-fABD2 after treatment with mock solution (0.1% DMSO), 10 µM CK-666, 25 µM SMIFH2, or both CK-666 and SMIFH2 for 5 min prior to imaging with VAEM. Actin filament arrays in CK-666-treated cells and SMIFH2-treated cells appeared to be less dense and less bundled compared to mock-treated cells. However, dual treatment markedly increased actin filament abundance. Bar = 10 µm. B, Quantitative analysis of actin filament nucleation frequency, both overall and by subclass of origin. The total nucleation frequency in mock-

treated cells was higher than CK-666-treated and SMIFH2-treated cells. However, the total nucleation frequency of dual-treated cells was significantly higher than other treatments and this correlated with increased *de novo* and side-branching nucleation events. Values in (B) represent mean ± SE. $n \geq 300$ total events from at least 10 hypocotyls per treatment (One-way ANOVA with Tukey's post-hoc test, letters [a–g] denote treatments that show statistically significant differences with other treatments, $P < 0.05$). C and D, Quantitative analysis of density (C) and skewness (D) of actin filaments. (C) The density of actin arrays in CK-666-treated and SMIFH2-treated cells was decreased compared to mock-treated cells; however, dual-treated cells had significantly increased actin density compared to other treatments. (D) Actin arrays in CK-666- or dual-treated cells were significantly less bundled than in mock-treated cells. Values in (C) and (D) represent mean ± SE. $n \geq 300$ ROIs from at least 15 hypocotyls per treatment (One-way ANOVA with Tukey's post-hoc test, letters [a–d] denote treatments that show statistically significant differences with other treatments, $P < 0.05$). All data shown are from one representative experiment of three biological repeats conducted with independent plant materials.